



Dependence of estimated precipitation frequency and intensity on data resolution

Di Chen¹ · Aiguo Dai^{1,2}

Received: 25 October 2016 / Accepted: 24 July 2017
© Springer-Verlag GmbH Germany 2017

Abstract Precipitation frequency (F) and intensity (I) are important characteristics that climate models often fail to simulate realistically. Their estimates are highly sensitive to the spatial and temporal resolutions of the input data and this further complicates the comparison between models and observations. Here, we analyze 3-hourly precipitation data on a 0.25° grid from two satellite-derived datasets, namely TRMM 3B42 and CMORPH_V1.0, to quantify this dependence of the estimated precipitation F and I on data resolution. We then develop a simple probability-based relationship to explain this dependence, and examine the spatial and seasonal variations in the estimated F and I fields. As expected, precipitation F (I) increases (decreases) with the size of the grid box or time interval over which the data are averaged, but the magnitude of this change varies with location, and is strongest in the tropics and weakest in the subtropics. Our simple relationship can quantitatively explain this dependence of the estimated F and I on the spatial or temporal resolution of the input data. This demonstrates that large differences in the estimated F and I can arise purely from the differences in the spatial or temporal resolution of the input data. The results highlight the need to have similar resolution in comparing two datasets or between observations and models. Our estimates show that extremely low frequencies (<1%) are seen over the subtropics while the highest frequencies (20–40%) are located

mostly over the tropics, and that the high frequency results from both longer and more frequent precipitation events. Precipitation intensity is more uniformly distributed than frequency. Strong correlations between the amount and frequency confirm the notion that the frequency plays a bigger role than intensity in determining precipitation variations.

Keywords Precipitation · Frequency · Intensity · Data resolution · Model evaluation

1 Introduction

Besides precipitation amount (A), other precipitation characteristics such as frequency (F , the percentage of time it precipitates) and intensity (I , the precipitation rate averaged over the precipitating time only) are also needed to fully characterize precipitation (Trenberth et al. 2003; Trenberth 2011). Precipitation frequency and intensity also play an important role in modulating soil moisture, runoff, evaporation, and surface heat fluxes over land (Qian et al. 2006; Trenberth 2011). Moreover, they can help validate cumulus and other parameterizations in numerical weather and climate models, which still have large deficiencies in simulating precipitation frequency and intensity even though the mean precipitation rate (i.e., $P \equiv A/\Delta t = F \times I$, where Δt is the time of accumulation) may look reasonable (e.g., Dai 2006; Sun et al. 2006; DeMott et al. 2007; Deng et al. 2007).

Previous studies (e.g., Arkin 1979; Kedem et al. 1990; Dai et al. 1999, 2007; Dai 2001a, b) have shown that precipitation spatial variations and its diurnal cycle are largely determined by how often it rains (i.e., the frequency) rather than how intense it rains (i.e., the intensity), with the intensity only having about half of the strength of the diurnal

✉ Aiguo Dai
adai@albany.edu

¹ Department of Atmospheric and Environmental Sciences,
University at Albany, State University of New York (SUNY),
Albany, NY 12222, USA

² National Center for Atmospheric Research (NCAR), Boulder,
CO, USA

cycle in the frequency and amount (Dai et al. 2007). Furthermore, precipitation frequency is dominated by light to moderate precipitation events, and it peaks in the precipitation centers over the tropical oceans, such as the inter-tropical convergence zone (ITCZ) and the western Pacific warm pool (Dai et al. 2001a). However, precipitation intensity identifies regions where intense storms tend to occur (Zipser et al. 2006), such as the subtropical latitudes of both North and South America, the Congo Basin and the Himalaya (Biasutti et al. 2011). At most rain-gauge stations over China, Lu et al. (2016) also found that precipitation frequency explains more variance of summer precipitation than precipitation intensity does when the drizzling days ($P \leq 2 \text{ mm/day}$) are excluded. Thus, precipitation frequency tends to play a bigger role than precipitation intensity in determining the spatial patterns, the diurnal cycle and the temporal variations of precipitation over the globe.

Another motivation for examining precipitation frequency and intensity is that these two characteristics are likely to behave differently under greenhouse gas-induced global warming, with the intensity expected to increase (by $\sim 7\%/\text{K}$ on average, mostly following water vapor increase rates) while the overall precipitation frequency is predicted to decrease (mostly for light-to-moderate precipitation) (Trenberth et al. 2003; Sun et al. 2007; Trenberth 2011; Lau et al. 2013; Pendergrass and Hartmann 2014a; Dai et al. 2017). This expected response is qualitatively consistent with analyses of historical data, albeit daily or monthly data were often used in these analyses (e.g., Lau and Wu 2007; Liu et al. 2009; Shiu et al. 2012; Ma et al. 2015). The exact physical processes underlying this frequency decrease are not well known, with two possible mechanisms explored in Dai et al. (2017), although analytically frequency has to decrease because $A = F \times I$, $dA/A = dF/F + dI/I$, and globally averaged $dA/A \approx 2\%/\text{K}$ (determined by energy balances, Pendergrass and Hartmann 2014b) and mean $dI/I \approx 7\%/\text{K}$ (Trenberth et al. 2003).

Estimating precipitation frequency and intensity over the globe (Petty 1995, 1997; Dai 2001a, b) is, however, not an easy task. It requires many years of data with high temporal resolution (e.g., hourly or 3-hourly data). Besides the contiguous United States (CONUS; Higgins et al. 1996), hourly or 3-hourly precipitation data from rain-gauge observations are usually unavailable to the research community. Because of this, high-resolution precipitation data sets derived from satellite observations (e.g., Joyce et al. 2004; Huffman et al. 2007; Liu 2015; Gehne et al. 2016) have been widely used to characterize precipitation F , I , and diurnal cycle (e.g., Dai et al. 2007; Zhou et al. 2008; Ellis et al. 2009; Biasutti et al. 2011; Biasutti and Yuter 2013). Because of a lack of data with sub-daily resolution, daily-mean precipitation rates from rain-gauges have also been widely used to study

precipitation frequency and intensity (e.g., Lu et al. 2016) and to evaluate model-simulated frequency and intensity (e.g., Sun et al. 2006). However, as we know that precipitation usually occurs only during a fraction of time in a day, the frequency and intensity estimated from daily data will differ from those estimated from hourly data, even though the wet-day frequency estimated from such data are still useful in some applications (e.g., Sun et al. 2006, 2007; Pendergrass and Hartmann 2014a).

The task to estimate precipitation frequency and intensity is also complicated by the fact that the calculated frequency and intensity values vary with the spatial and temporal resolutions of the data used (Chen et al. 1996; Dai 2006). As the temporal aggregation increases, frequency values increase while intensity values decrease (Sun et al. 2006; Biasutti and Yuter 2013). Furthermore, the frequency and intensity depend on the thresholds used to define the precipitating events, with higher thresholds being associated with lower frequency and higher intensity (Zhou et al. 2008). With the increase in the threshold, the importance of frequency increases, while the importance of intensity decreases in determining local precipitation variability (Lu et al. 2016). Other earlier studies (e.g., Kedem and Chiu 1987; Kedem et al. 1990) have explored the spatial scale dependence of rain rates at some select locations.

Given the importance of studying precipitation frequency and intensity and the difficulties in reliably estimating them, here we analyze 3-hourly precipitation data on a 0.25° grid from two satellite-derived datasets to (1) explicitly quantify the dependence of the calculated precipitation frequency and intensity on the spatial and temporal resolutions of the input data, (2) explain this dependence using a simple relationship derived purely from probability considerations, and (3) examine the spatial and seasonal variations in our best estimates of precipitation frequency and intensity over the globe. Results from this study should improve our understanding of the resolution-dependence of estimated precipitation frequency and intensity and facilitate proper comparisons of them between models and observations.

The paper is organized as follows. Section 2 first describes the data sets and analysis method. In Sect. 3, precipitation amount, frequency and intensity over CONUS and the globe from the two satellite datasets are compared and evaluated against other rain-gauge and satellite products. The resolution-dependence of the calculated frequency and intensity and its statistical explanation are presented in Sect. 4. Section 5 describes the spatial and seasonal variations in precipitation frequency and intensity based on our best estimates. A summary and conclusions are presented in Sect. 6.

2 Data and method

Details of the data sets used in this study are listed in Table 1 with references and web links. The two main products are the blended precipitation data from TRMM 3B42 (Huffman et al. 2007) and CMORPH_V1_ADJ (Xie et al. 2017), both are 3-h averaged (referred to as 3-hourly) precipitation on a 0.25° grid. CMORPH uses precipitation estimates derived from low-orbit satellite microwave observations, whose features are interpolated in time via spatial propagation using geostationary satellite infrared (IR) images (Joyce et al. 2004). CMORPH_V1_ADJ is a bias-adjusted version of the CMORPH dataset through PDF matching with daily rain gauge data over land and pentad GPGP precipitation over oceans (Xie et al. 2017). However, even after the bias correction (mainly through re-scaling), there is still an underestimation for cold-season precipitation in this dataset, because current microwave-based precipitation retrievals are very poor in depicting snowfall (set to zero, which was multiplied by a constant during the bias correction) during the cold season (Xie and Joyce 2014). On the other hand, the TRMM 3B42 forcefully adjusted the satellite estimates up to the magnitude indicated by monthly gauge analysis from the Global Precipitation Climatology Centre (GPCC). Therefore, differences between CMORPH and TRMM 3B42 are expected, especially for winter precipitation.

Dai et al. (2007) showed that spatial patterns in the mean precipitation amount from the TRMM 3B42 and CMORPH datasets are comparable to other monthly products like GPCP v2.2 (Huffman et al. 2009). Here we used the GPCP v2.2 and the Climate Prediction Center (CPC) hourly precipitation data over CONUS (Table 1) to further evaluate the TRMM 3B42 and CMORPH_V1_ADJ products over the globe and CONUS, respectively. The GPCP v2.2 (with ~38,000–10,000 stations from 1998–present) and CPC (with 2500–2900 stations) precipitation data over land were derived primarily from gauge observations and thus are likely to be more reliable than the satellite products. The 3-hourly precipitation amount from TRMM and CMORPH datasets was simply averaged onto the coarse grids of the GPCP and CPC products and also over a common time period in the comparison. The CPC hourly precipitation was averaged to 3-hourly data to be compatible with the satellite products.

After the evaluation, the TRMM and CMOPRH 3-hourly precipitation data on a 0.25° grid, together with their averaged versions on coarser grids at 0.5° , 1.0° and 2.0° , were analyzed to investigate the dependence of the estimated precipitation frequency and intensity on the spatial resolution of the input data. To examine their dependence on temporal resolution of the data, the 3-hourly precipitation from the TRMM and CMORPH products were added up

Table 1 Precipitation data sets and sources

Dataset name (reference)	Resolution and coverage	Data sources and merging method	Online documentation
TRMM 3B42 (Huffman et al. 2007)	0.25° grid, 50°S – 50°N , 180°W – 180°E ; 3-hourly, 1/1998–present	Microwave (TRMM, SSM/I, AMSR and AMSU) precipitation estimates were used to adjust IR estimates from geostationary IR observations. The rainfall estimates were scaled to match the monthly rain-gauge analysis used in TRMM 3B-43	http://disc.sci.gsfc.nasa.gov/precipitation/documentation/TRMM_README/TRMM_3B42_readme.shtml
CMORPH_V1_ADJ (Joyce et al. 2004; Xie et al. 2017)	0.25° grid, 60°S – 60°N , 180°W – 180°E ; 3-hourly, 1/1998–present	Microwave estimates from the DMSP 13, 14 and 15 (SSM/I), the NOAA-15, 16 and 17 (AMSU-B) and the TRMM (TMI) satellites are propagated by motion vectors derived from geostationary satellite infrared data	https://ftp.cpc.ncep.noaa.gov/precip/CMORPH_V1.0/CRT/
CPC Hourly U.S. Precipitation (Higgins et al. 1996)	2.5° lon \times 2.0° lat, 20°N – 60°N , 140°W – 60°W ; hourly, 7/1948–10/2002	Hourly reports from ~2800 rain gauges were used to derive the gridded data	http://www.esrl.noaa.gov/psd/data/gridded/data.cpc_hour.html
GPCP v2.2 (Huffman et al. 2009)	2.5° grid, globe, monthly, 1979–2014	Over regions without rain gauge data, IR estimates were calibrated by microwave estimates and then adjusted by rain-gauge data	http://precip.gsfc.nasa.gov/

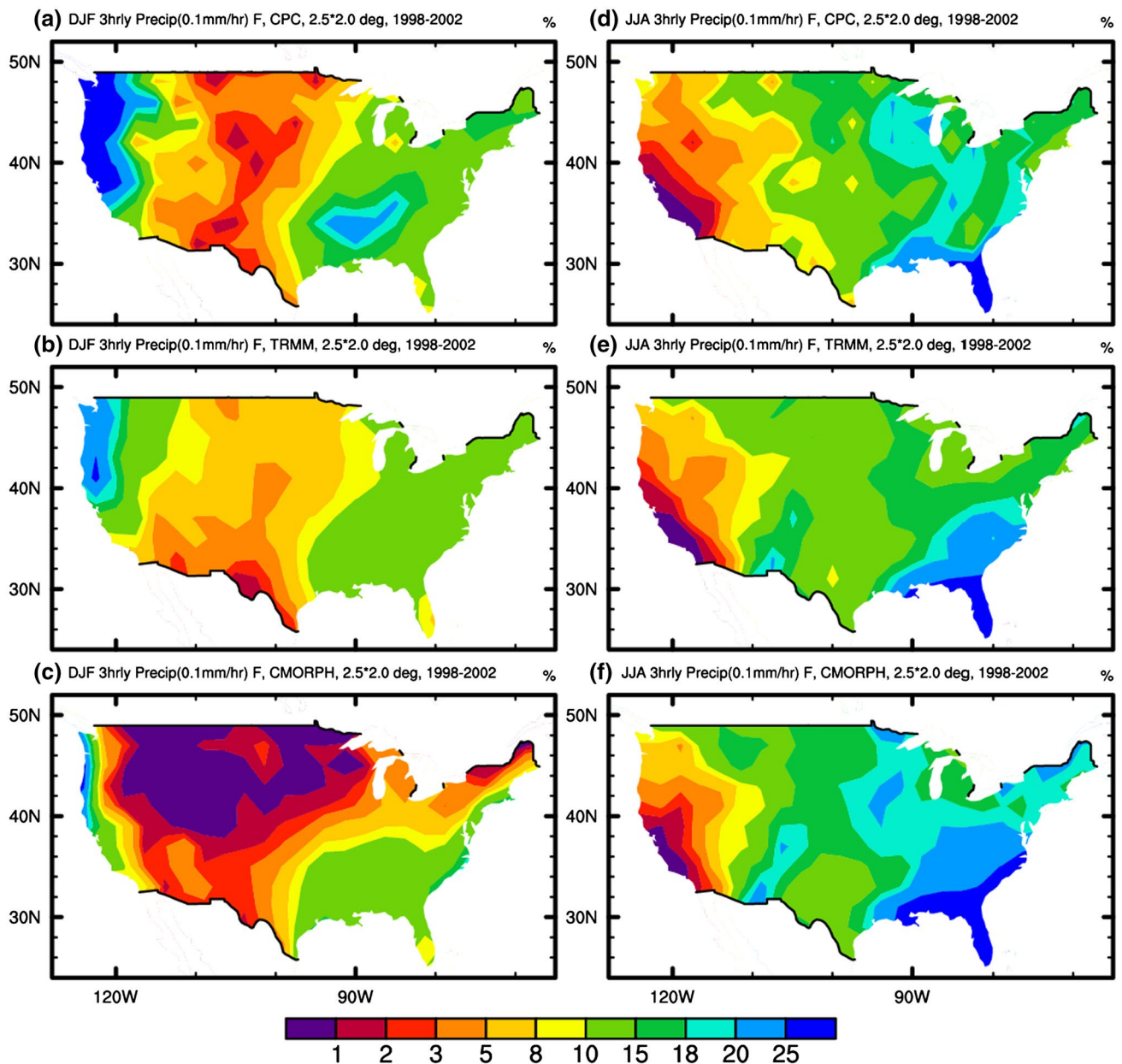


Fig. 1 1998–2002 mean DJF (left) and JJA (right) precipitation frequency (%) based on 3-hourly data over the contiguous U.S. derived from (top) CPC gauge analysis, (middle) TRMM 3B42 and (bottom) bias-adjusted CMORPH. TRMM 3B42 and adjusted CMORPH data

were averaged to the same $2.5^\circ \times 2.0^\circ$ grid as the CPC data (which were averaged from hourly to 3-hourly values). Precipitation events were defined as any 3-h periods with a precipitation rate exceeding 0.1 mm/h

to produce 6-hourly, 12-hourly and daily mean precipitation rates. Then, the precipitation frequency and intensity estimated using the 3-hourly, 6-hourly, 12-hourly and daily precipitation rates were compared to quantify the dependence on the temporal resolution of the input data.

For calculating precipitation frequency and intensity, here a precipitation event is defined as a time period (e.g., a 3-h period for 3-hourly data, or a day for daily data) with a precipitation rate larger than certain criterion (e.g.,

$P > 0.1 \text{ mm/h}$ or 1 mm/day). The frequency is the number of the precipitation events expressed as a percentage of the total number of observations, and the intensity is the mean precipitation rate averaged over all precipitation events. The frequency and intensity were computed at each grid box for each season or the whole year for each year and then averaged over all the years with data within the period from 1998–2014. Similar methods were used in previous studies (e.g., Dai 2001; Dai 2006; Dai et al. 2007).

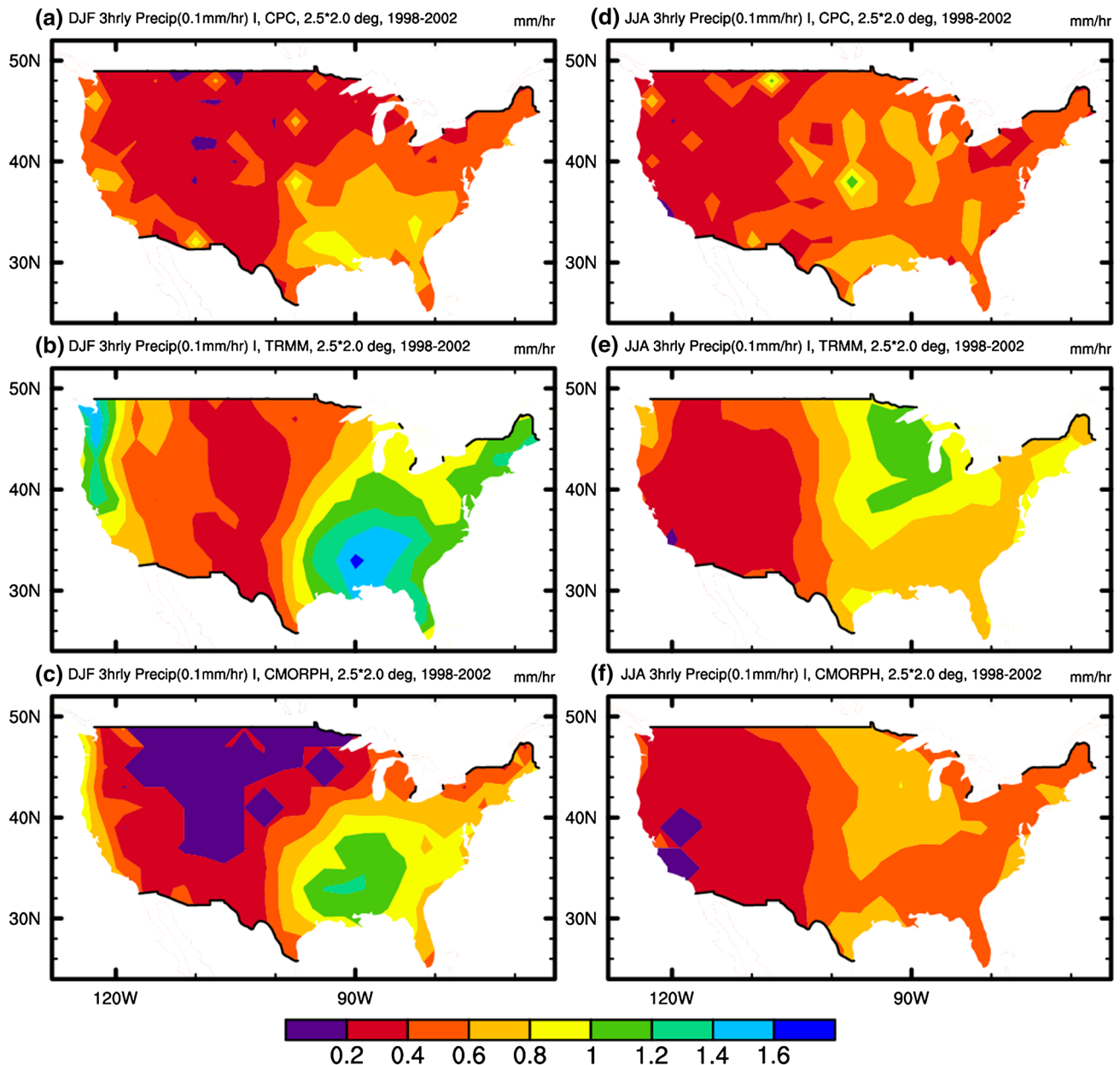


Fig. 2 Same as Fig. 2 but for precipitation intensity (in mm/h)

To help understand and explain the dependence of the estimated precipitation frequency and intensity on data resolution, we developed a simple statistical relationship in “Appendix” based on basic probability concepts. As shown below, this simple relationship can quantitatively explain the resolution dependence seen in our calculations using the TRMM and CMORPH data. This demonstrates that averaging precipitation rates over different spatial and temporal scales can lead to different values of the estimated frequency and intensity simply due to the

changing probability of precipitation over different spatial and temporal scales.

3 Comparison of the precipitation products

We first compare the multi-year mean December–February (DJF) and June–August (JJA) precipitation amount (not shown) from GPCP v2.2, TRMM 3B42 and CMORPH_V1_ADJ. Although substantial differences are evident, large-scale patterns are comparable among these

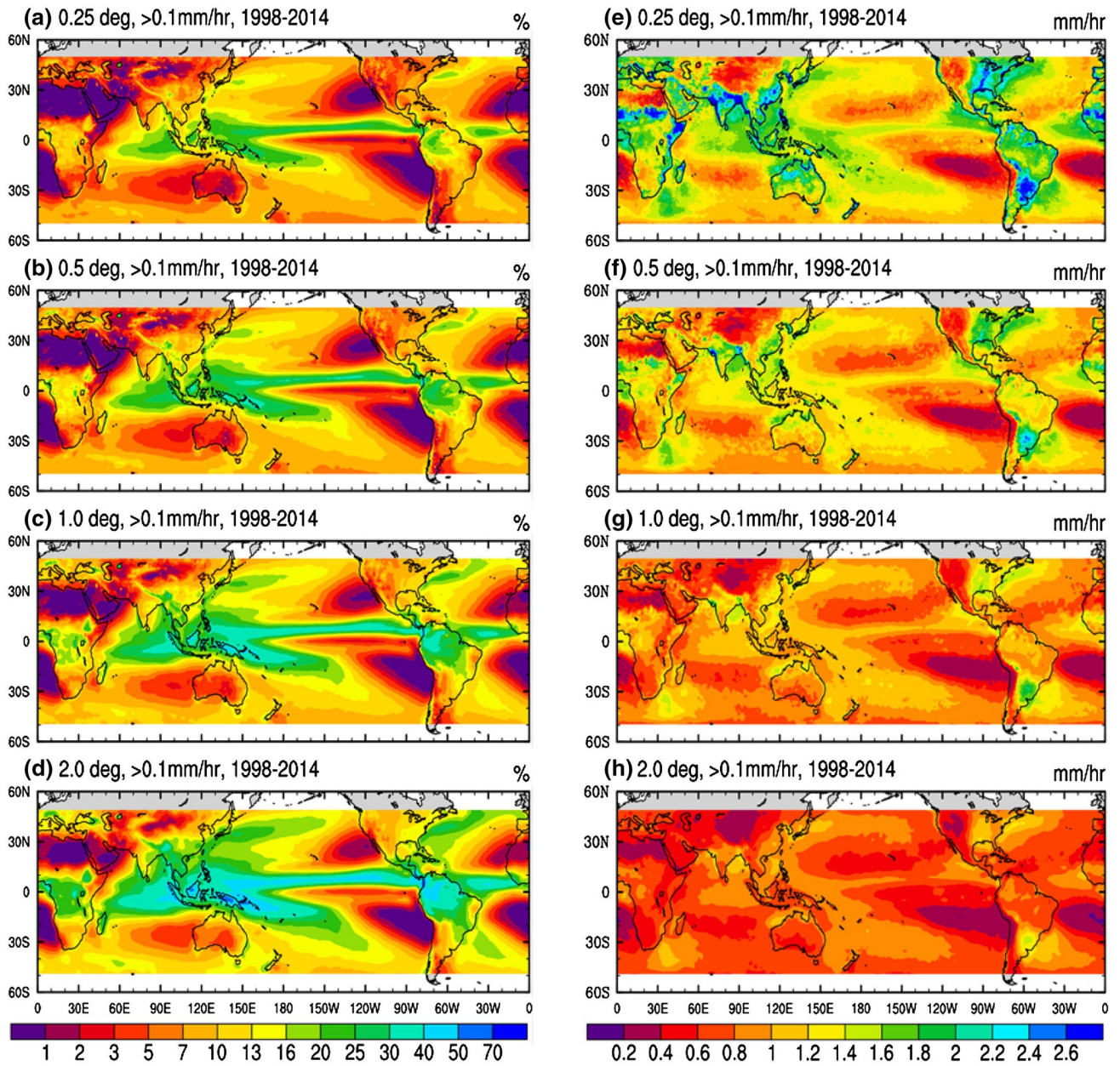


Fig. 3 1998–2014 mean annual precipitation (>0.1 mm/h) frequency (left panels) and intensity (right panels) estimated using TRMM 3B42 3-hourly data on four different grids

three products, as shown in many previous analyses (e.g., Gehne et al. 2016; Xie et al. 2017). However, CMORPH cold-season precipitation is unrealistically too low over many northern mid-high latitude land areas due to problems in satellite observations of snowfall, as mentioned in Sect. 2. Therefore, CMORPH cold-season precipitation over the northern mid-high latitude land are unreliable and should not be used, as stated in the CMORPH documentation (Xie and Joyce 2014).

Figure 1 compares the 1998–2002 mean DJF and JJA precipitation frequency (with $P > 0.1$ mm/h as the cutoff criterion) estimated using 3-hourly data on a $2.5^\circ \times 2.0^\circ$ grid derived from the CPC hourly dataset, TRMM 3B42 and CMORPH_V1_ADJ. Except the snowfall-related problem in the CMORPH DJF data, overall they agree reasonably well, with the east coast and southeast U.S. having high frequency in both DJF and JJA and the southwest coast having the lowest frequency (<2%) in JJA (Fig. 1). During winter, precipitation frequency over the west coast (~25%)

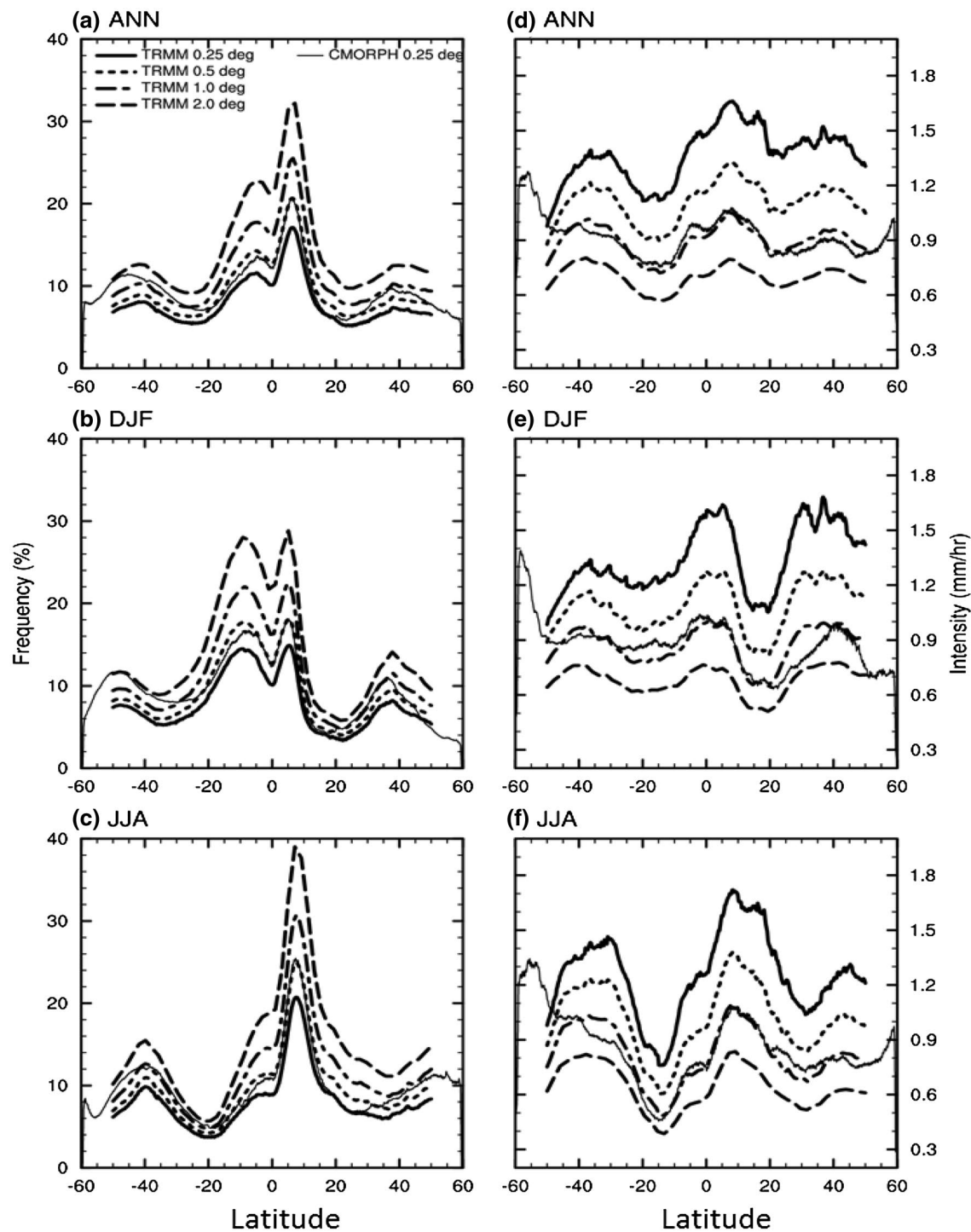


Fig. 4 Zonal-mean precipitation ($>0.1 \text{ mm/h}$) frequency (%), *left*) and intensity (mm/h, *right*) estimated using TRMM 3B42 3-hourly data on four different grids and the CMORPH_V1_ADJ 3-hourly data on 0.25° grid (thin solid line)

and the lower Mississippi river basin ($\sim 15\text{--}20\%$) is higher in the CPC dataset than the TRMM and CMORPH datasets, while the lowest DJF frequency ($\sim 1\text{--}3\%$) is seen along $100^\circ\text{--}110^\circ\text{W}$ in both the CPC and TRMM datasets (Fig. 1a,

b). Again, CMORPH_V1_ADJ failed to capture DJF precipitation over inland areas north of $\sim 35^\circ\text{N}$ in the central and western U.S. During summer, CMORPH_V1_ADJ overestimates the frequency over the southeast U.S., while

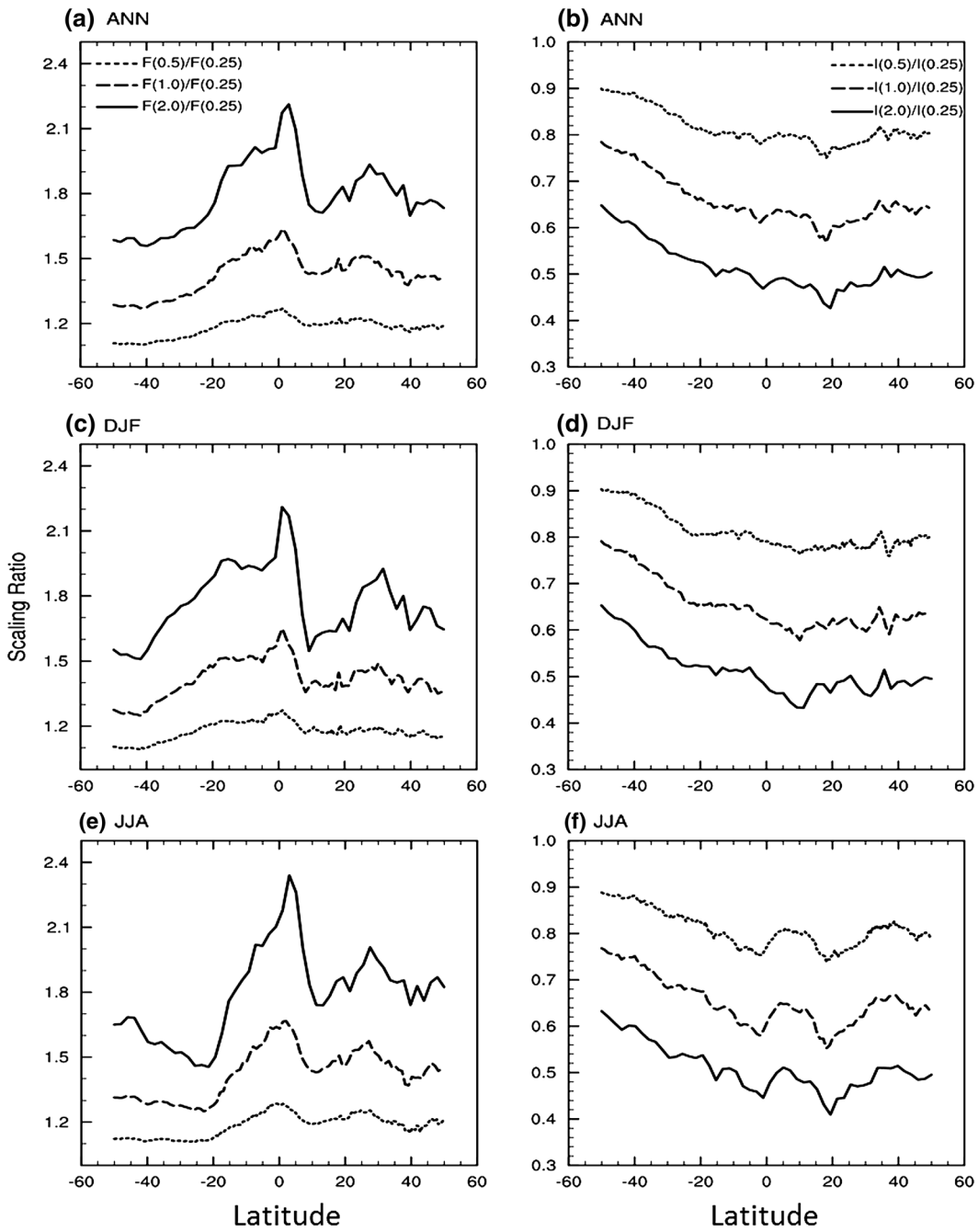


Fig. 5 The ratio of zonal-mean frequency (**a, c, e**) and intensity (**b, d, f**) estimated using TRMM3B42 1998–2014 data on coarser grids to those estimated using the data on 0.25° grid

TRMM 3B42 slightly underestimates the frequency around the Great Lakes.

The corresponding precipitation intensity is shown in Fig. 2. The intensity is generally lower over the western U.S. in the three datasets. However, TRMM 3B42 overestimates the intensity east of about 98°W for both DJF and JJA, especially for the Southeast in DJF and the Midwest

for JJA. The CMORPH_V1_ADJ also overestimates the DJF intensity over the lower Mississippi river basin, reflecting the negative biases in the frequency (Fig. 1).

In summary, TRMM 3B42 shows spatial patterns of precipitation amount comparable to GPCP v2.2, except slightly lower precipitation over the tropical western Pacific and northeastern North Pacific, and slightly higher

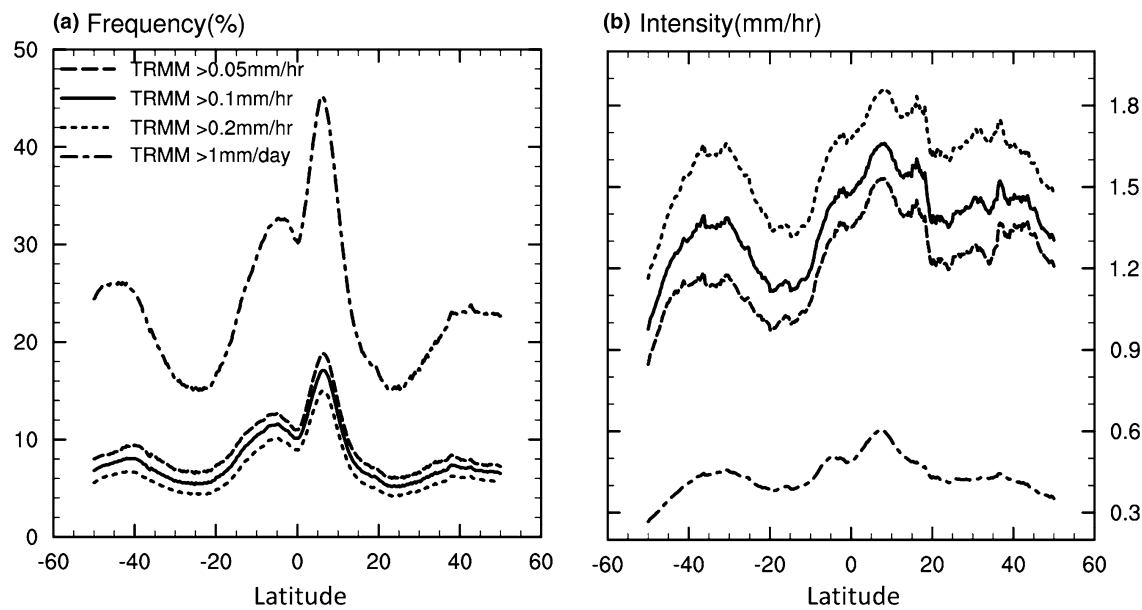


Fig. 6 Zonal-mean precipitation frequency and intensity estimated using TRMM 3B42 data on the 0.25° grid with four different cutoff thresholds (daily data were derived from the 3-hourly data for the $P > 1 \text{ mm/day}$ case)

estimates over the tropical Indian Ocean. Precipitation frequency and intensity over the U.S. calculated from TRMM 3B42 are broadly comparable to those based on CPC gauge data, with somewhat lower frequency and higher intensity over the southeast U.S. On the other hand, CMORPH_V1_ADJ does not capture DJF precipitation well over northern mid-high latitude land, including the inland central and western U.S., due to problems with snowfall. During summer, CMORPH_V1_ADJ is fairly consistent with GPCP v2.2 and the CPC gauge data. These comparisons revealed substantial uncertainties among the existing precipitation products as found by others (e.g., Gehne et al. 2016), and this will affect the estimated frequency and intensity results discussed in Sect. 5. However, we believe that the TRMM 3B42 is realistic enough for quantifying the dependence of the estimated precipitation frequency and intensity on data resolution (Sect. 4). Because the problem with cold-season precipitation in CMORPH_V1_ADJ, TRMM 3B42 will be our main dataset used in Sect. 4.

4 Dependence of precipitation frequency and intensity on data resolution

4.1 Dependence on spatial resolution

Figure 3 shows the 1998–2014 mean annual precipitation frequency and intensity estimated using TRMM 3B42 3-hourly data (with a cutoff threshold of $P > 0.1 \text{ mm/h}$)

averaged onto four different grids: 0.25° (original grid), 0.5° , 1.0° and 2.0° . It is clear that the spatial patterns in the frequency fields are correlated with those in the precipitation amount ($r = 0.93$), but the pattern correlation between the intensity and amount is weak ($r = 0.04$), which confirms the previous notion (Kedem et al. 1990; Dai 2001a; Dai et al. 2007) that the frequency contributes more than the intensity to the spatial variations of precipitation as mentioned in Introduction. This is not inconsistent with Arkin (1979), who showed that the areal rainfall amount is determined by its fractional coverage for a given region over the Atlantic, since the fractional coverage reflects the occurrence frequency of precipitation over a region.

As expected, Fig. 3 shows that the frequency (intensity) increases (decreases) substantially as the data are averaged over increasingly larger areas, except for deserts and subtropical oceans where precipitation rarely occurs. For example, the frequency over the Pacific ITCZ increases from ~20–25% on the 0.25° grid to ~25–30% on the 0.5° grid, ~30–35% on the 1.0° grid, and ~35–45% on the 2.0° grid (Fig. 3a–d). The changes in the intensity is also large, for example, from ~1.6 mm/h on the 0.25° grid to ~1.0 mm/h on the 2.0° grid over the Pacific ITCZ (Fig. 3e, h). The increases in the frequency and decreases in the intensity with the averaging size are seen at all latitudes (Fig. 4), with the resolution-dependence being strongest in the tropics and weakest in the subtropics presumably due to the persistent dry conditions there.

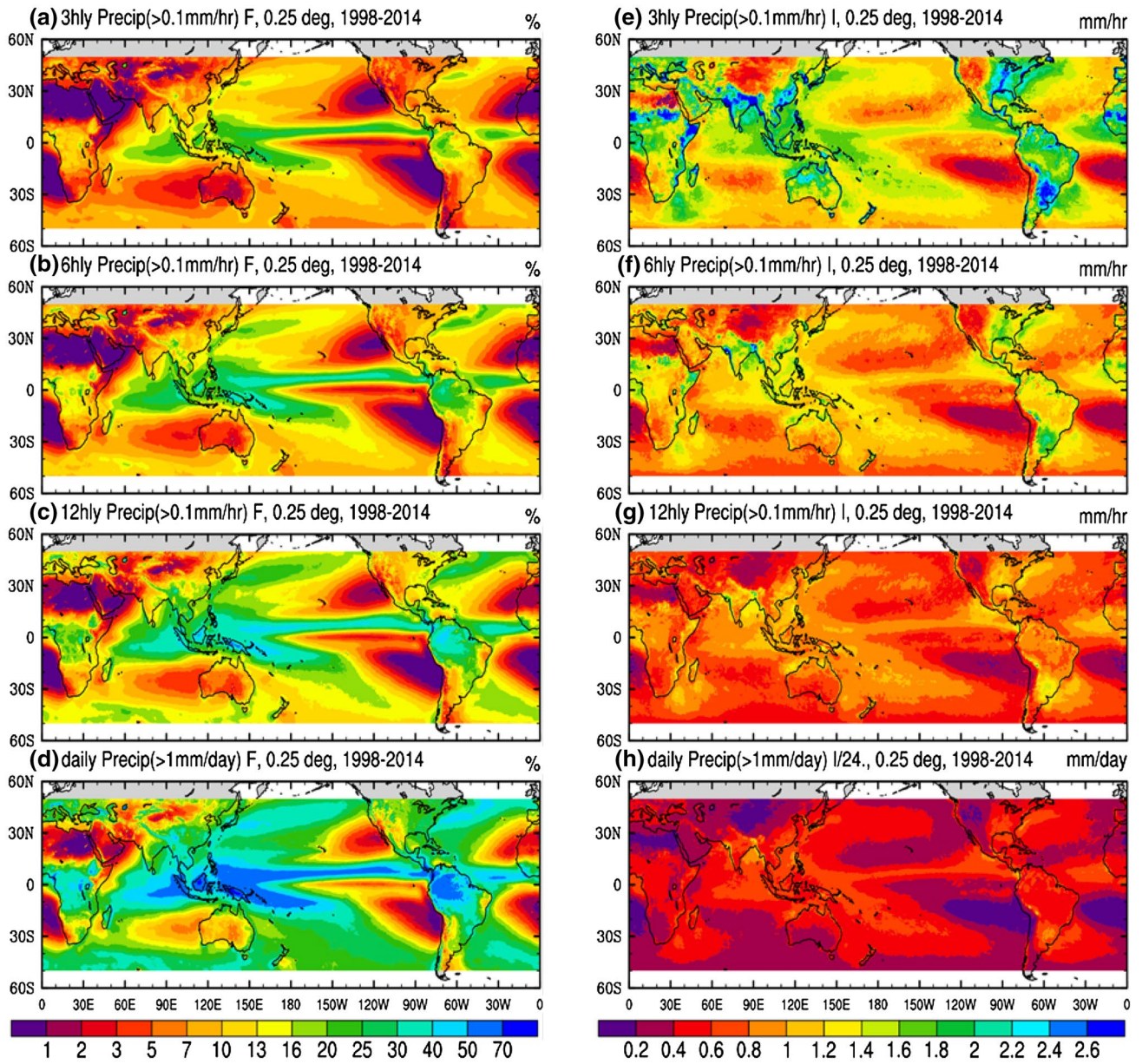


Fig. 7 1998–2014 mean annual precipitation frequency (%; left) and intensity (mm/h; right) calculated using TRMM 3B42 data averaged onto four different temporal resolutions on the same 0.25° grid: **a, e** 3-hourly, **b, f** 6-hourly, **c, g** 12-hourly, and **d, h** daily. The $P > 0.1$ mm/h threshold was used for all cases except the daily case where $P > 1$ mm/day was used

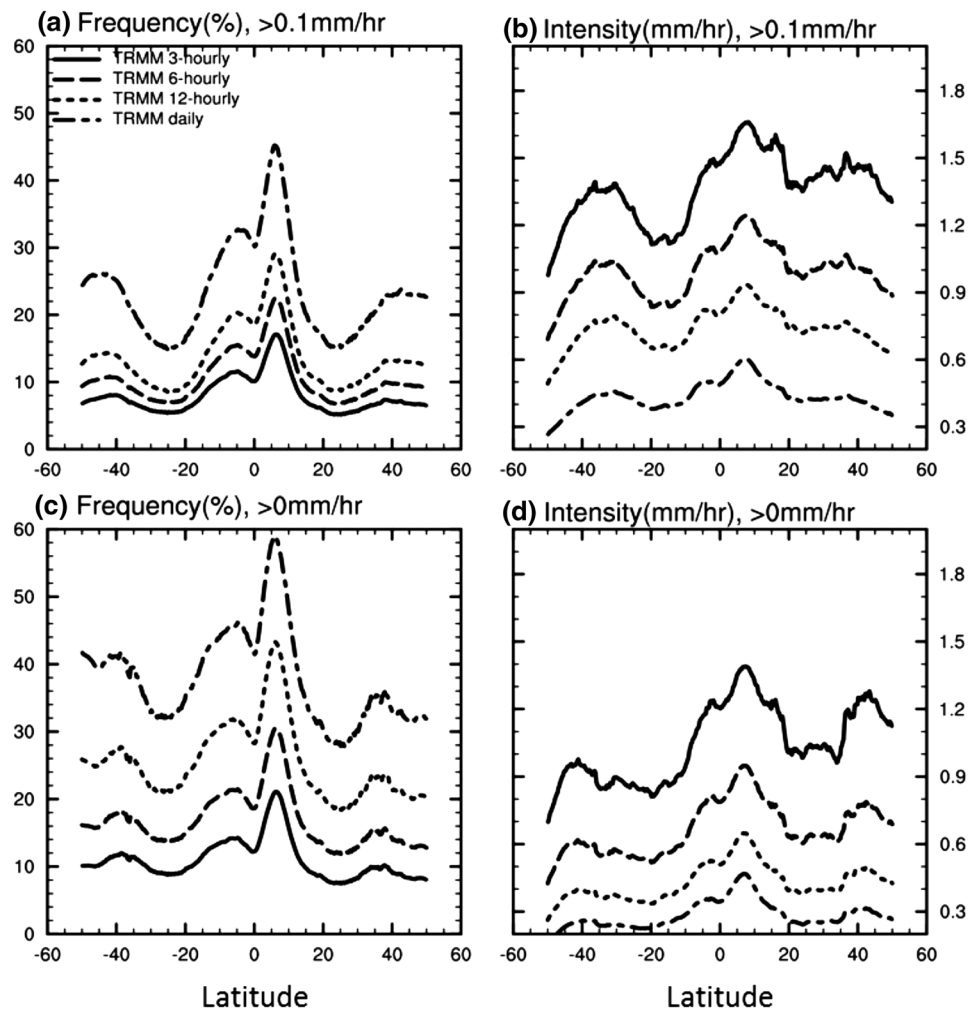
Figure 5 shows the ratio of the zonal-mean frequency or intensity derived on a coarse grid to that derived on the original 0.25° grid. These ratios may be used as an approximate scaling factor to convert the frequency and intensity estimates using data on different grids (e.g., 1° and 2°) onto a common grid (e.g., 0.25°) to facilitate the comparison. Figure 5 shows that this scaling factor varies with latitude, i.e., it is not a constant that one might expect it to be related to the ratio of the grid box area on the two grids if the precipitation events are uncorrelated spatially (i.e., random in space, see “Appendix”). The spatial variations in this

scaling ratio is related to the spatial correlation distance of precipitation that varies with location (Bell et al. 1990; Dai et al. 1997). This ratio ranges from about 2.4 in the ITCZ to around 1.5 in the subtropics for the frequency on 2.0° grid, and from 1.1 to 1.3 for the frequency on 0.5° grid.

4.2 Dependence on temporal resolution

Before analyzing the dependence on temporal resolution, we first examine the sensitivity of the estimated frequency and intensity on the cutoff threshold used to define

Fig. 8 Zonal-mean annual precipitation, **a** frequency and **b** intensity estimated using TRMM 3B42 data on the 0.25° grid on four different temporal resolutions and the same thresholds as shown in Fig. 7. **c**, **d** Same as **a**, **b**, except for using the $P > 0$ threshold for all cases



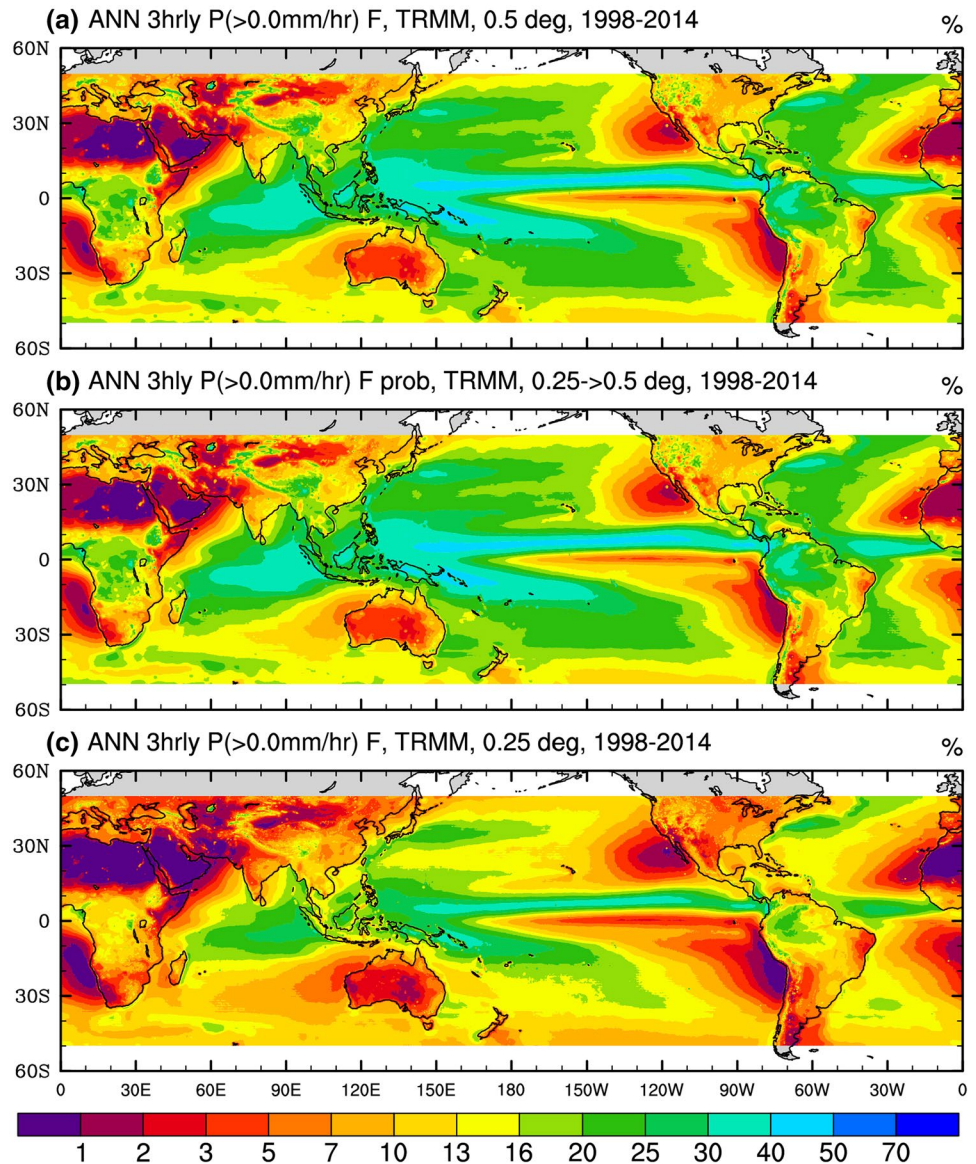
precipitation events. Note that all calculations in this subsection were on the 0.25° grid. Figure 6 shows the zonally-averaged frequency and intensity calculated using 3-hourly data from TRMM 3B42 with three different thresholds: $P > 0.05$, 0.1 , or 0.2 mm/h, and for $P > 1$ mm/day using daily data (derived from the 3-hourly data). As expected, the frequency (intensity) decreases (increases) as the cut-off threshold increases, but only slightly for the first three cases. However, the commonly used threshold of $P > 1$ mm/day for daily data (e.g., Dai 2006; Sun et al. 2006) yields much higher frequency (by ~ 3 times) than that derived using the 3-hourly data with thresholds around 0.1 mm/h (Fig. 6a), while the intensity is just the opposite (Fig. 6b). Thus, the frequency and intensity calculated using daily data (e.g., Sun et al. 2006, 2007; Lu et al. 2016) are not comparable to those estimated using 3-hourly data. In this study, we chose the $P > 0.1$ mm/h threshold for 3-hourly data for most calculations. While the estimated precipitation amount may also depend on the cutoff threshold (Kedem et al. 1990), its sensitivity to the threshold is much

lower than that for the frequency and intensity shown in Fig. 6.

Figure 7 compares the annual-mean precipitation frequency and intensity calculated using the TRMM 3B42 data averaged onto four different temporal resolutions from 3-hourly to daily. As the temporal resolution decreases, precipitation frequency increases while intensity decreases substantially, similar to that shown in Fig. 3 for the dependence on spatial resolution. Overall, the daily frequency is about 2–3 (not $24/3=8$ as for a random process) times higher than the 3-hourly frequency, consistent with Fig. 6. For instance, the precipitation frequency over the Pacific ITCZ is around 20% for the 3-hourly case (Fig. 7a), but it increases to ~ 50 – 60 % for the daily precipitation case (Fig. 7d). The dependence on the temporal resolution is shown more clearly in the zonal-mean frequency and intensity (Fig. 8), which again reveals relatively small (large) sensitivity over the subtropics (tropics).

One may wonder that as the averaging time period changes, the equivalent cutoff threshold may change as

Fig. 9 1998–2014 mean annual precipitation frequency estimated **a** directly from TRMM 3B42 3-hourly data averaged onto the 0.5° grid, and **b** using the TRMM data on the 0.25° grid and applying the probability-based model (Eq. 4 in “[Appendix](#)”). Also shown **c** is the precipitation frequency estimated using the data on 0.25° grid. The threshold of $P > 0$ was applied for all cases



well. To avoid this problem, we repeated the calculations with a threshold of $P > 0$. For this setup, the threshold should be the same for all the resolution cases. The results (Fig. 8c, d) reveal similar dependence of the frequency and intensity on the data averaging period, with generally higher frequency and lower intensity than the positive threshold cases as one would expect.

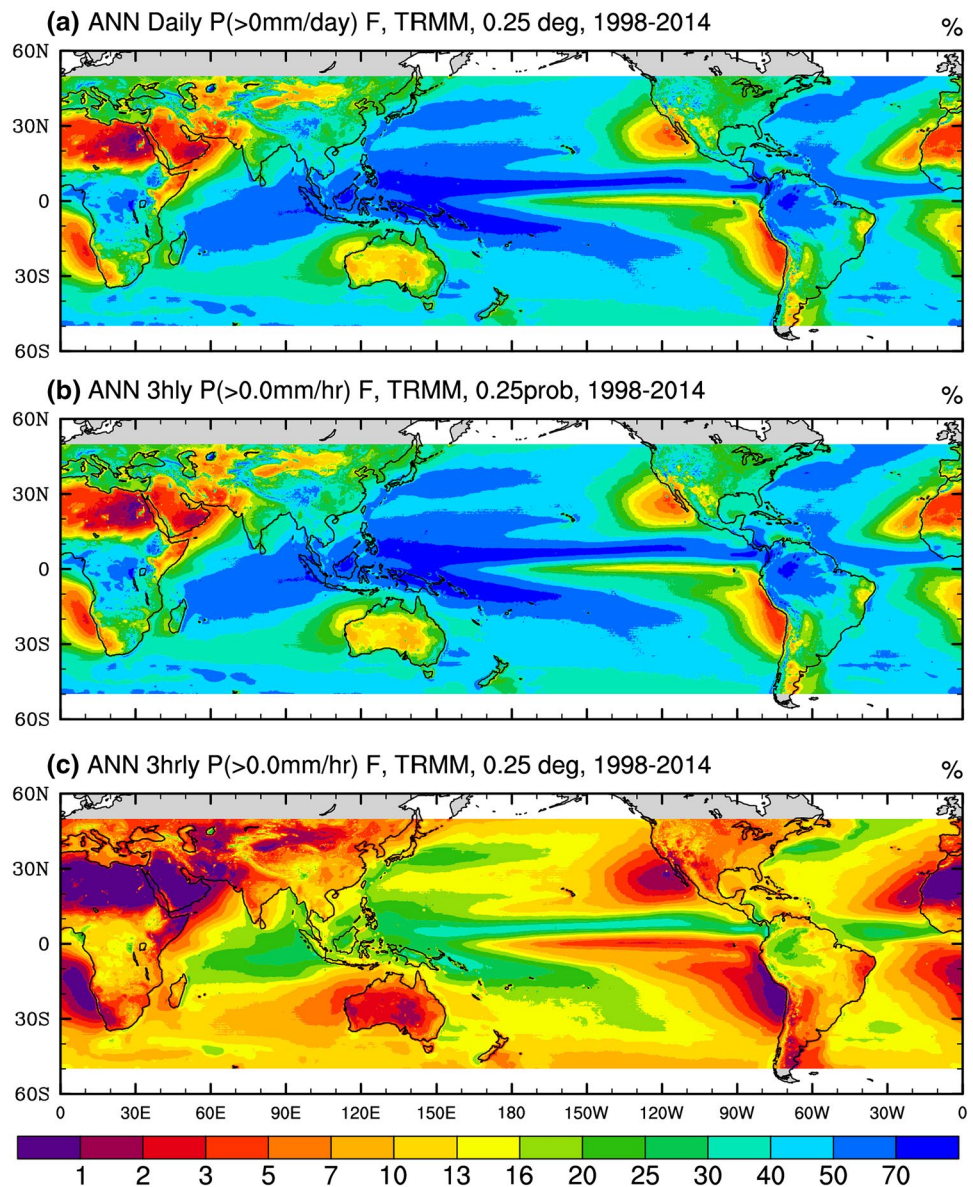
4.3 Probability-based explanation

To help understand and quantitatively explain the dependence of the estimated frequency and intensity on the spatial and temporal resolution of the input data, we have developed a simple relationship based on pure probability considerations (see “[Appendix](#)”). The use of this relationship is to demonstrate that the resolution dependence discussed

above can be entirely explained by probability theory through a simple relationship such as the one described in “[Appendix](#)”. Here we compare the frequency map estimated directly from the TRMM 3B42 data (direct estimate) and that estimated using the simple relationship (model estimate) based purely on probability considerations. To avoid the issue of the equivalent threshold that may change with data resolution, in this subsection we simply use the $P > 0$ threshold for all calculations, which allows a more accurate comparison between the direct and model estimates.

Figure 9a shows the frequency estimated directly from the TRMM data averaged onto the 0.5° grid, similar to Fig. 3b but for the threshold of $P > 0$ mm/h rather than $P > 0.1$ mm/h, thus it shows higher frequency than Fig. 3b as drizzling events with $0 < P \leq 0.1$ mm/h are also included

Fig. 10 1998–2014 mean annual daily precipitation frequency estimated from **a** daily mean precipitation rates derived from TRMM 3B42, and **b** 3-hourly TRMM 3B42 data and the Eq. (5) in “[Appendix](#)”. Also shown (**c**) is the precipitation frequency estimated using the 3-hourly data. The threshold of $P > 0$ was applied for all cases



in Fig. 9a. To verify whether the estimated frequency on the 0.25° and 0.5° grids are related quantitatively following our simple relationship described in “[Appendix](#)”, we used the TRMM data on the 0.25° grid and Eq. (4) in “[Appendix](#)” to derive another estimate of the frequency on the 0.5° grid, which is shown in Fig. 9b. Clearly, the two estimates are nearly identical everywhere. Similar to Fig. 3, the estimated frequency using the data on the 0.5° grid (Fig. 9a) is considerably higher than that on the 0.25° grid (Fig. 9c), and this increase of precipitation frequency with grid size can be quantitatively explained purely based on probability considerations (Fig. 9b) as described in “[Appendix](#)”. While this finding is not surprising, Fig. 9 does confirm that our simple relationship works as expected and provides a quantitative link between the frequencies estimated

on two different grids. This link shows that the increase of the estimated frequency with grid size results purely from the increased probability of precipitation over a larger area. Thus, one should expect to see some differences between the estimated precipitation frequency (and intensity) using observational and model data when the data are on different grids, even if the model is perfect.

Similarly, Fig. 10 compares the frequency estimated directly using daily mean rates (derived from the TRMM 3B42 3-hourly data), using the 3-hourly data (Fig. 10c) and a simple relationship (Eq. 5 in “[Appendix](#)”) (Fig. 10b). It is evident that the two estimates are nearly identical, suggesting that the increase with the averaging time period for the estimated precipitation frequency (i.e., from Fig. 10a–c) can also be explained entirely based on occurrence

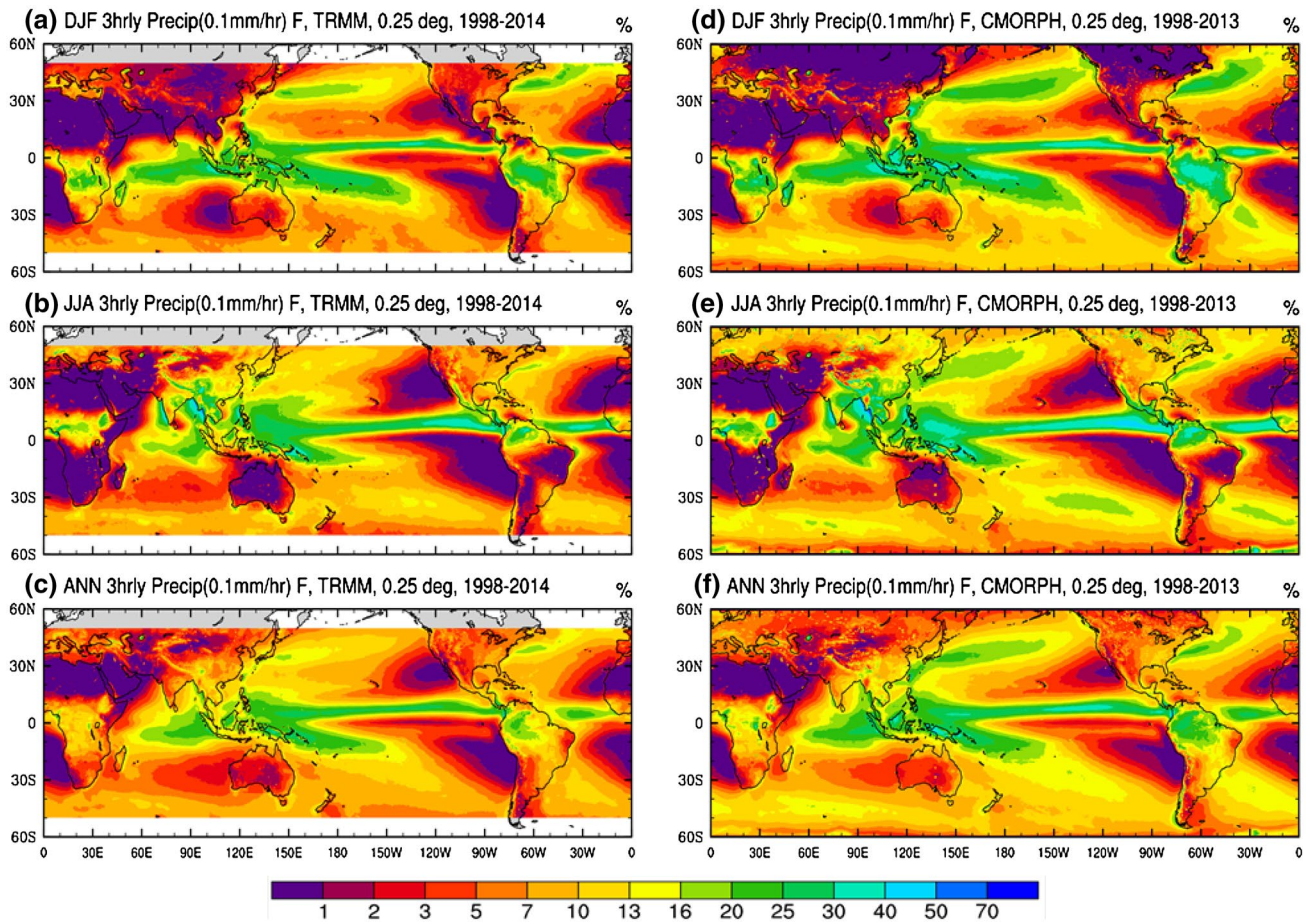


Fig. 11 1998–2014 mean (*top*) DJF, (*middle*) JJA, and (*bottom*) annual precipitation frequency (%) from **a–c** TRMM 3B42 and **d–f** CMORPH_V1_ADJ, which is problematic for DJF over mid-high latitude land

probability considerations (i.e. Fig. 10b). While this is expected, Fig. 10 proves that Eq. (5) in “Appendix” correctly describes the link between the frequencies estimated using daily and 3-hourly data.

5 Seasonal and spatial variations in precipitation frequency and intensity

In this section, we describe the major features in seasonal and spatial variations of precipitation frequency and intensity based on the 3-hourly data on a 0.25° grid (Figs. 11, 12). As shown above (e.g., Fig. 3), the magnitude of the frequency and intensity depends on the data resolution, but the spatial patterns remain the same. Thus, we will focus on the patterns. For quantitative comparison, one needs to use the scaling factor of Fig. 5 to convert the frequency and intensity onto similar spatial resolution, and Fig. 8 to convert them onto similar temporal resolution for the input data. We cannot conclude which of the two datasets is more realistic in depicting the precipitation frequency (besides

the DJF snowfall issue), although the TRMM 3B42 appears to perform slightly better than the CMORPH dataset in comparison with the CPC gauge data over the U.S. Thus, we show the frequency and intensity maps from both datasets here.

Figure 11 shows that regions with extremely low frequency (<1%) are seen over the subtropical regions, such as the Mediterranean region (including the Middle East and northern Africa), the eastern part of the subtropical Pacific and Atlantic Ocean, and winter Australia and southern Africa. The highest frequencies (20–40%) are located over the ITCZ in the Pacific and Atlantic, the western Pacific warm pool, the South Pacific Convergence Zone (SPCZ), and summer South Asia and the Bay of Bengal (Fig. 11). Other land areas typically have a frequency below 10% (lower in winter and higher in summer). The CMORPH_V1_ADJ dataset generally shows higher frequencies than TRMM 3B42 over both ocean and land (except winter mid-latitude and high latitudes due to the snowfall issue).

To help us understand the frequency patterns, we computed the duration of continuous light precipitation

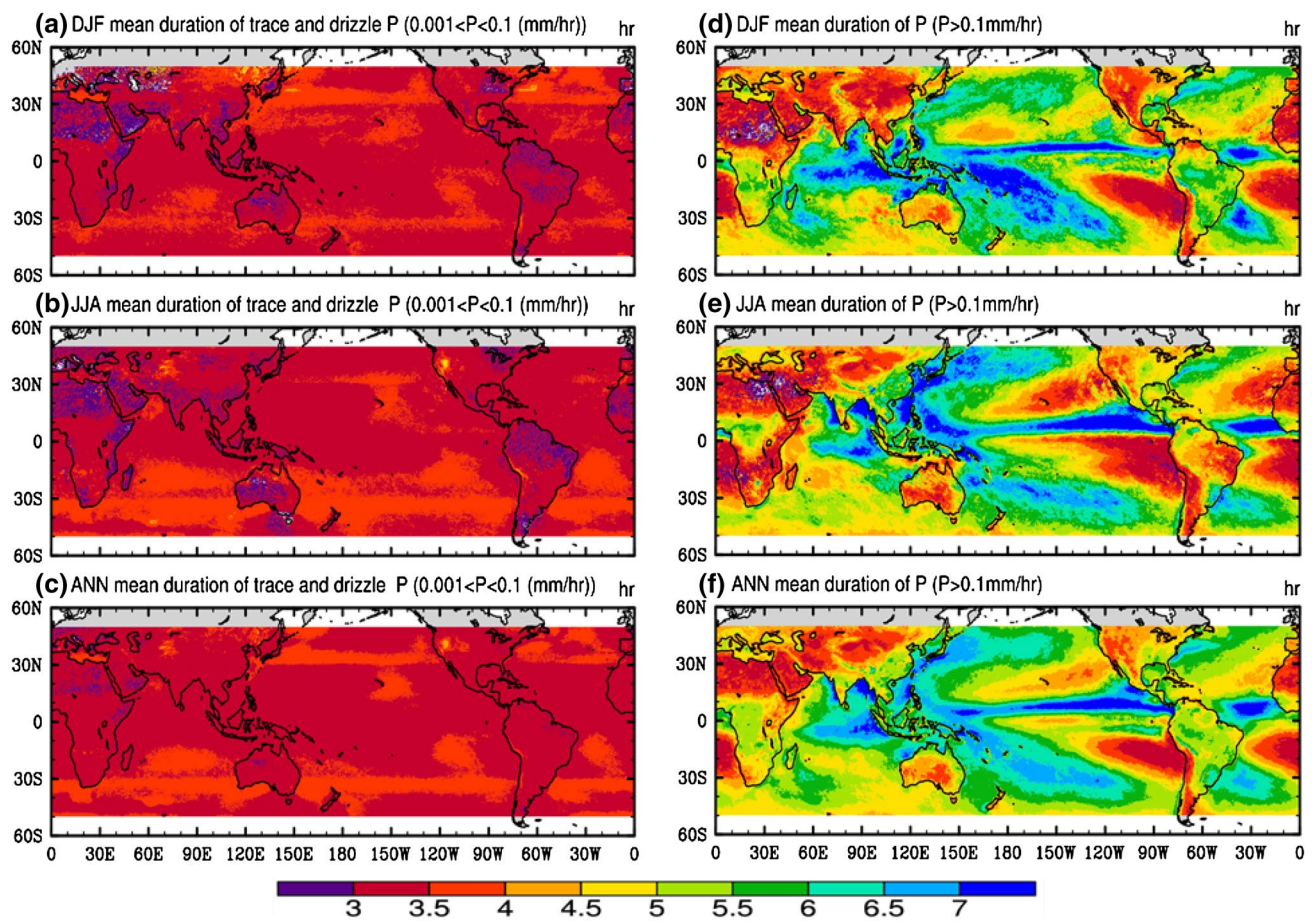


Fig. 12 1998–2014 mean (*top*) DJF, (*middle*) JJA, and (*bottom*) annual precipitation duration (hours) of continuous **a–c** light precipitation ($0.05 \text{ mm/h} < P < 1 \text{ mm/h}$) events and **d–f** all precipitation events with $P > 0.1 \text{ mm/h}$ estimated using 3-hourly data from TRMM

3B42 on a 0.25° grid. The pattern correlation coefficient between the mean duration (**d–f**) and the corresponding frequency maps (Fig. 11d–f) is 0.78, 0.79 and 0.78 for DJF, JJA and ANN, respectively

($0.05 < P < 1.0 \text{ mm/h}$) events and of all precipitation events with $P > 0.1 \text{ mm/h}$ using the 3-hourly TRMM 3B42 data on its 0.25° grid. Figure 12 shows that the mean duration of light precipitation events is between 3.0 and 4.0 h over most land areas and between 3.5 and 4.5 h over most oceans with only small seasonal variations. The mean duration of all precipitation events with $P > 0.1 \text{ mm/h}$ exhibits spatial patterns (Fig. 12d–f) that are similar to those of precipitation frequency (Fig. 11a–c), with a pattern correlation coefficient of ~ 0.78 . The longest rain events ($\sim 7\text{--}8 \text{ h}$) tend to occur in the ITCZ, the western Pacific and parts of the Indian Ocean, while precipitation events over land and subtropical oceans areas tend to have much shorter durations ($\sim 3\text{--}4 \text{ h}$) (Fig. 12d–f). The duration for the light-moderate ($0.1 < P < 2.0 \text{ mm/h}$) and heavy ($> 2.0 \text{ mm/h}$) events (Fig. 13) usually last shorter than 4–5 h. However, the duration of $P > 0.1 \text{ mm/h}$ events can last longer than 4–5 h (Fig. 12d–f). This suggests that many of these

3-hourly precipitation events (with $P > 0.1 \text{ mm/h}$) can change intensity (e.g., from heavy to light-moderate rates) during their lifetime.

By dividing the mean precipitating time over a 24-h period ($=24 \times$ frequency) by the mean duration, we can derive the mean number of (continuous) precipitation events per 24-h period. The spatial pattern of this mean event number (Fig. 14) is also very similar (pattern correlation ≈ 0.97) to that of the frequency (Fig. 11a–c), with the highest values ($\sim 1.0\text{--}1.2 \text{ events/day}$) in the tropical rain centers over South America and Africa and high values ($\sim 0.7\text{--}1.0 \text{ events/day}$) in the tropical convergence zones and northern midlatitude storm track regions in DJF (Fig. 14a, b). Thus, on average precipitation occurs every day in these regions. In contrast, most winter land areas, northern Africa and the Middle East have on average one precipitation event in more than 10 days. These results show that the high precipitation frequency in the tropical convergence zones and northern storm track regions (Fig. 11a, b) results

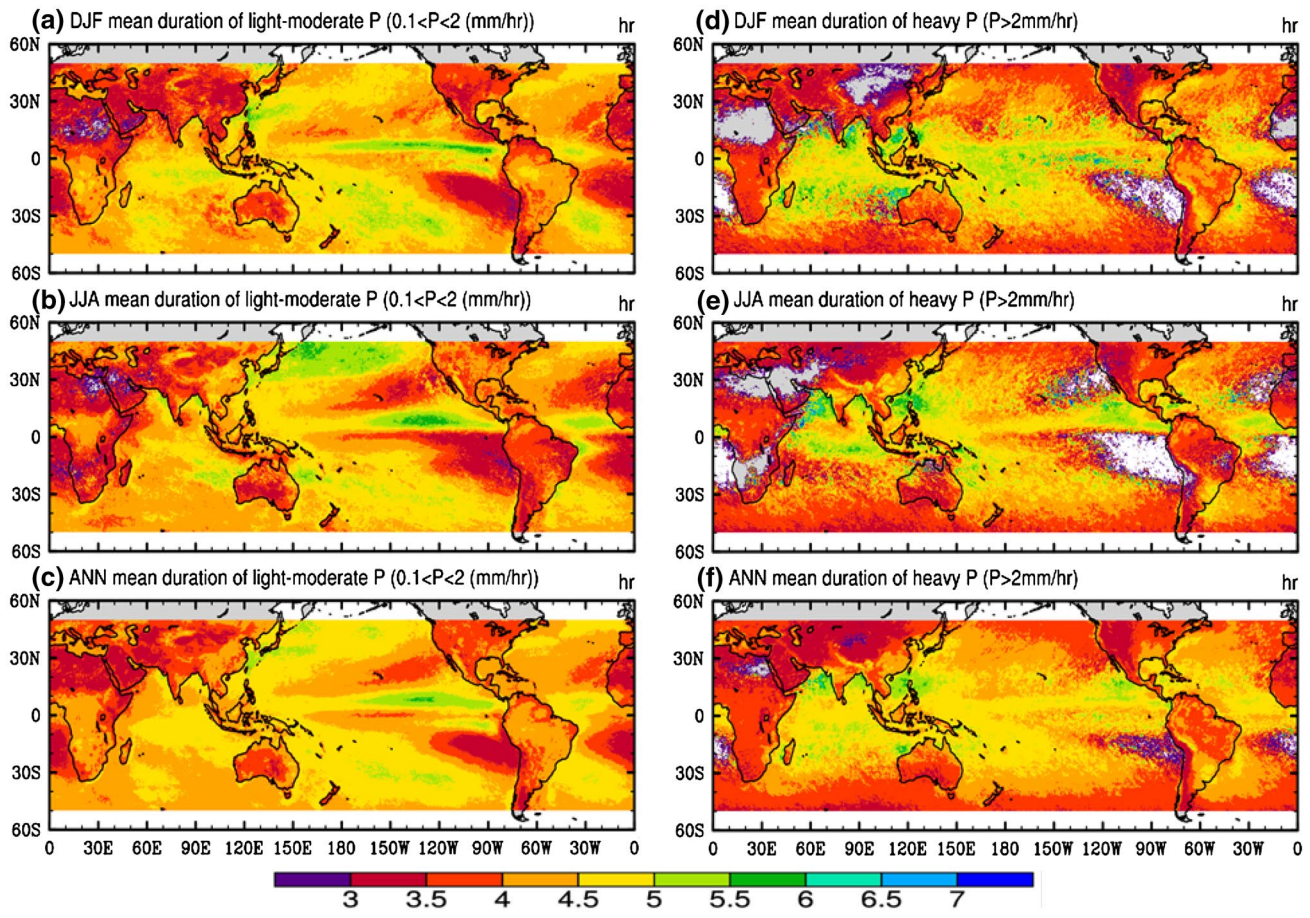


Fig. 13 Same as Fig. 12 but for the mean duration of **a–c** light-moderate ($0.1 < P < 2 \text{ mm/h}$) and **d–f** heavy ($P > 2.0 \text{ mm/h}$) precipitation events

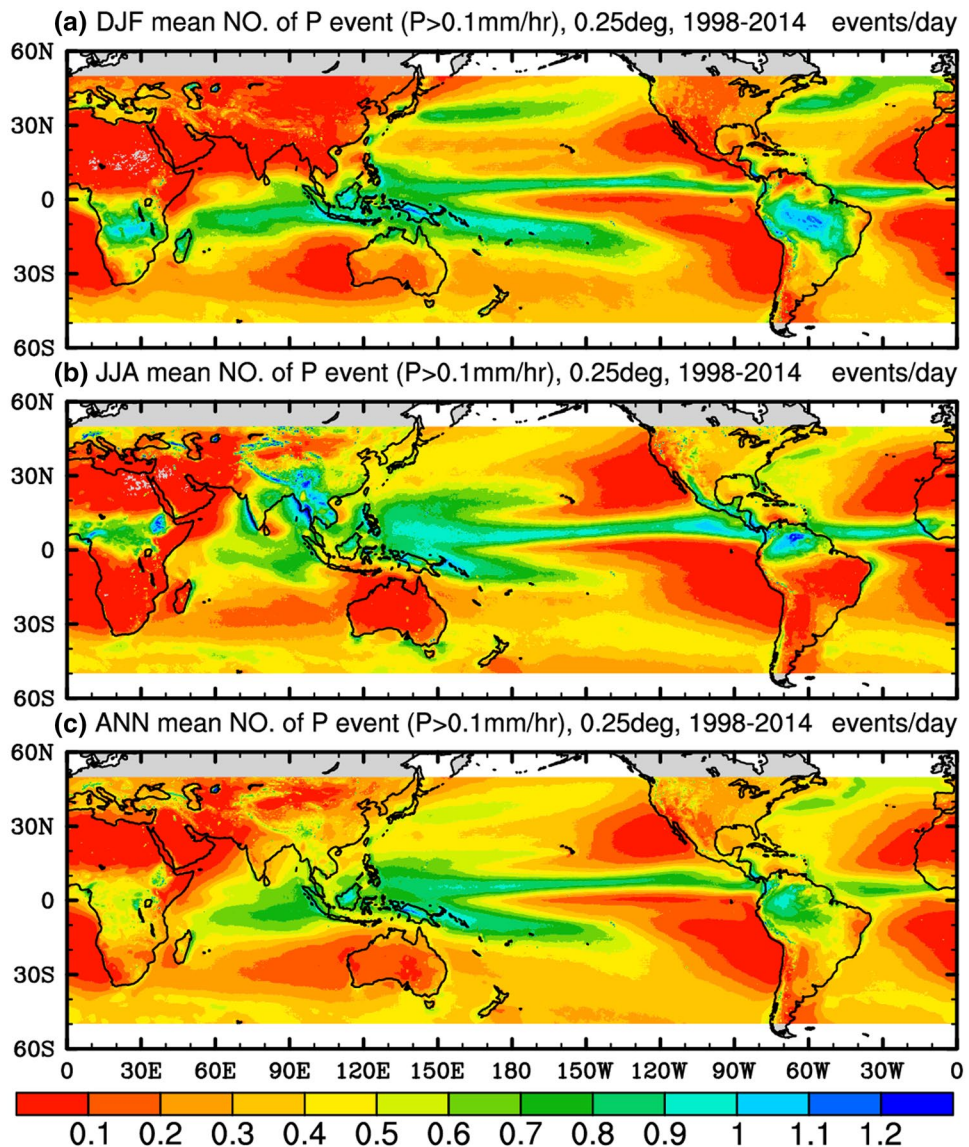
not only from longer but also more frequent precipitation events.

The lower frequency for the TRMM dataset leads to higher intensity (by 0.1–0.5 mm/h) in comparison with the CMORPH dataset over both land and ocean (Fig. 15). The intensity shows a broad region of relatively high values of 1.8–2.4 mm/h (for TRMM, or 1.2–1.6 for CMORPH) from South Asia to Australia and the tropical western Pacific. The intensity is also relatively high over South America and eastern North America (Fig. 15). In general, the intensity is more uniformly distributed than the frequency, especially over the oceans, and its seasonal variations are also smaller than those of the frequency (Figs. 11, 15). For example, the intensity over Australia, around 1.6–2.2 mm/h (for TRMM), is similar for both DJF and JJA, but its frequency (Fig. 11) and thus its precipitation amount are much lower during JJA than DJF.

Annual cycles of zonal-mean precipitation amount, frequency, and intensity are shown in Fig. 16, which shows similar seasonal variations among them although

the location of the May–November position of the ITCZ is linked more closely to precipitation frequency than intensity. Again, the magnitude of the seasonal variations is larger for frequency (from 2 to 20%, a factor of 10) than for intensity (from 0.6 to 1.8 mm/h, a factor of 3). The tropics are characterized by relatively high precipitation amount (3–8 mm/day), high frequency (8–20%) and high intensity (1.2–1.8 mm/h) all year round (Fig. 16). The subtropics and mid-latitudes show large seasonality, with lower amount, frequency and intensity during winter. As the ITCZ and monsoon move to the summer hemisphere, precipitation amount, frequency and intensity peak during this time of the year. The frequency evolution resembles the amount better than the intensity, which is consistent with the notion that precipitation amount is more dependent on frequency than intensity (Dai et al. 1999, 2007; Dai 2001a, b). Nevertheless, over 30° – 45° N the frequency does not show large seasonal variations (Fig. 16b) and the intensity is the main driver for the seasonal variations in precipitation amount at these latitudes

Fig. 14 1998–2014 mean (top) DJF, (middle) JJA, and (bottom) annual precipitation ($P > 0.1 \text{ mm/h}$) event number per 24 h period estimated using 3-hourly data from TRMM 3B42 on a 0.25° grid. The event number is defined as $24 \text{ h} \times \text{frequency} \div \text{duration}$. The pattern correlation coefficient with the corresponding frequency maps (Fig. 11d–f) is 0.98, 0.96 and 0.97, and with the duration maps (Fig. 12d–f) is 0.70, 0.69 and 0.69 for DJF, JJA and ANN, respectively



with more precipitation and higher intensity from October–March (Fig. 16a, c).

To examine the contributions of the frequency (F) and intensity (I) to the year-to-year variations in precipitation amount (A), Fig. 17 shows the local correlations between monthly anomalies of A and F, and A and I, as well as between F and I. Correlations for individual seasons are similar with slightly weaker and noisier F-I correlations (not shown). Since $A = F \times I$, positive A-F and A-I correlations are expected, although the strength may vary. Furthermore, F and I are not physically linked in general, thus the F-I correlations are expected to be much weaker. Figure 17 generally confirms these expectation. Precipitation amount is strongly correlated with frequency, with the correlation coefficient (r) exceeding 0.7 over most of the

globe; and the strongest correlations ($r=0.9\text{--}1.0$) are seen over arid northern Africa and the Middle East and northern China, as well the low-latitude Atlantic and Pacific Ocean (Fig. 17a). The correlation between the amount and intensity (Fig. 17b) is significant ($r=0.5\text{--}0.8$) over most of the oceans and many land areas, but it is noticeably weaker than that between the amount and frequency. This is consistent with the notion that precipitation frequency plays a bigger role than intensity in determining the variability of precipitation amount. The amount vs. intensity correlation is insignificant over a number of regions, such as northern Africa and several land areas in Southeast and central Asia, central South America, and the western U.S. (Fig. 17b). This suggests that changes in the number of precipitation events essentially determine annual precipitation amount

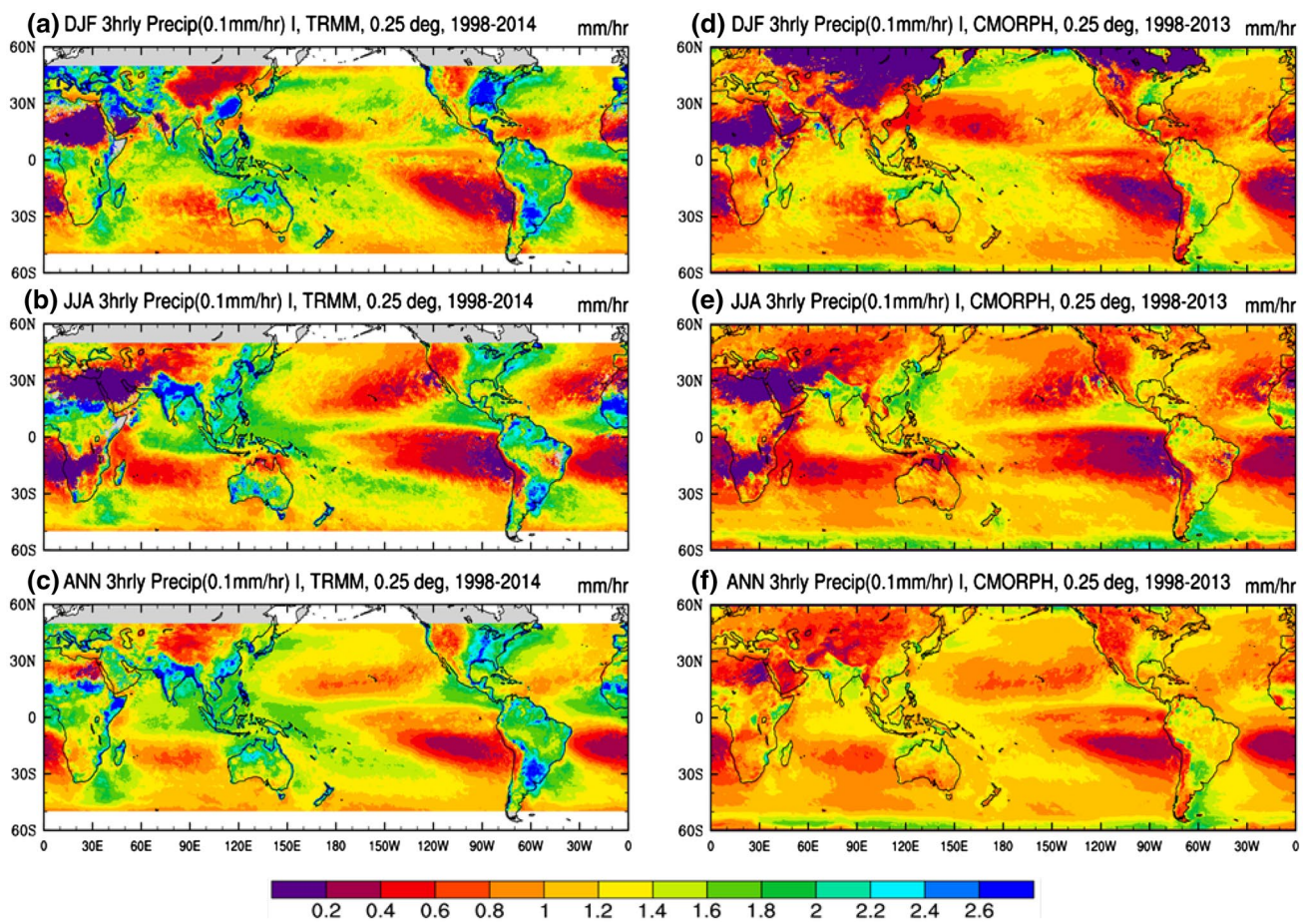


Fig. 15 1998–2014 mean (*top*) DJF, (*middle*) JJA, and (*bottom*) annual precipitation intensity (mm/h) from **a–c** TRMM 3B42 and **d–f** CMORPH_V1_ADJ, which is problematic for DJF land

over these arid regions, consistent with results based on station data (Sun et al. 2006). There exist considerable correlations ($r=0.3\text{--}0.7$) between the frequency and intensity over most of the low-latitude oceans and parts of Asia, southern African and northern Australia, while the correlation is weak outside the $30^{\circ}\text{S}\text{--}30^{\circ}\text{N}$ zone and it is negative over the Southeast U.S., the Sahel, and parts of Southeast and central Asia, and Europe (Fig. 17c). The negative F-I correlations suggest that increased precipitation events tend to occur with light intensity (e.g., during the cold season), while the positive F-I correlations imply that more precipitation events tend to occur with high intensity (e.g., during the monsoon season over Asia). The exact relationship between F and I requires further investigation.

6 Summary and conclusions

We have used the 3-hourly precipitation data from TRMM 3B42 and CMORPH_V1_AJD to estimate precipitation

frequency and intensity and examined their dependence on the spatial and temporal resolution of the input data. A simple relationship was developed to quantitatively explain this dependence based on basic probability concepts. Major features in the spatial and seasonal variations of precipitation frequency, intensity and duration were examined, together with their contributions to precipitation variability. Main results are summarized below.

The satellite-based TRMM 3B42 dataset shows spatial patterns of precipitation amount that are comparable to GPCP. Precipitation frequency and intensity calculated from TRMM 3B42 are generally comparable to those estimated using CPC rain gauge data. However, CMORPH_V1_AJD does not capture snowfall at northern latitudes in winter, making it unsuitable for cold-season precipitation at these latitudes.

As expected, the estimated precipitation frequency increases with the averaging spatial and temporal size of the input data, while the intensity decreases with the averaging size. Using data on a 0.25° grid, the estimated

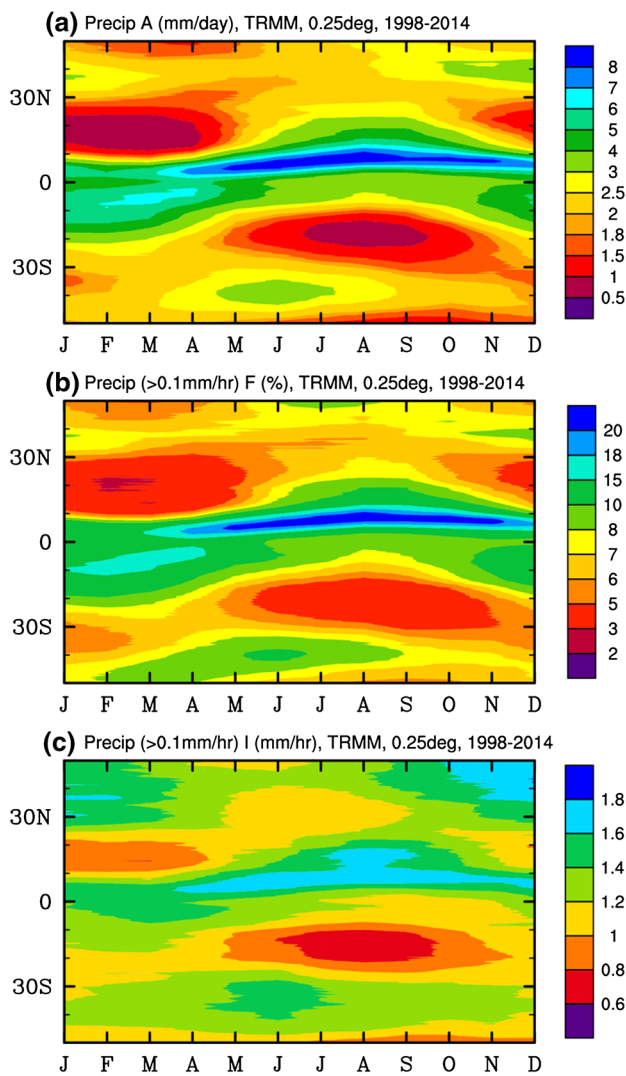


Fig. 16 Annual cycle of zonal-mean precipitation **a** amount, **b** frequency and **c** intensity. The data used is TRMM 3B42 3-hourly precipitation on a 0.25° grid, and the time period is from 1998 to 2014. The cutoff threshold is 0.1 mm/h

annual frequency peaks at $\sim 25\%$ over the Pacific ITCZ, and it increases to $\sim 40\%$ when data on a 2.0° grid are used. In contrast, the intensity for the Pacific ITCZ decreases from about $1.4\text{--}1.6 \text{ mm/h}$ using data on a 0.25° grid to about 1.0 mm/h using data on a 2.0° grid. This dependence is strongest in the tropics and weakest in the subtropics. Similar to the dependence on spatial averaging, precipitation frequency increases and intensity decreases substantially as the data averaging time period increases. Using daily precipitation with a threshold of $P > 1 \text{ mm/day}$ yields much higher frequency (by ~ 3 times) than that derived using 3-hourly data with a threshold around 0.1 mm/h .

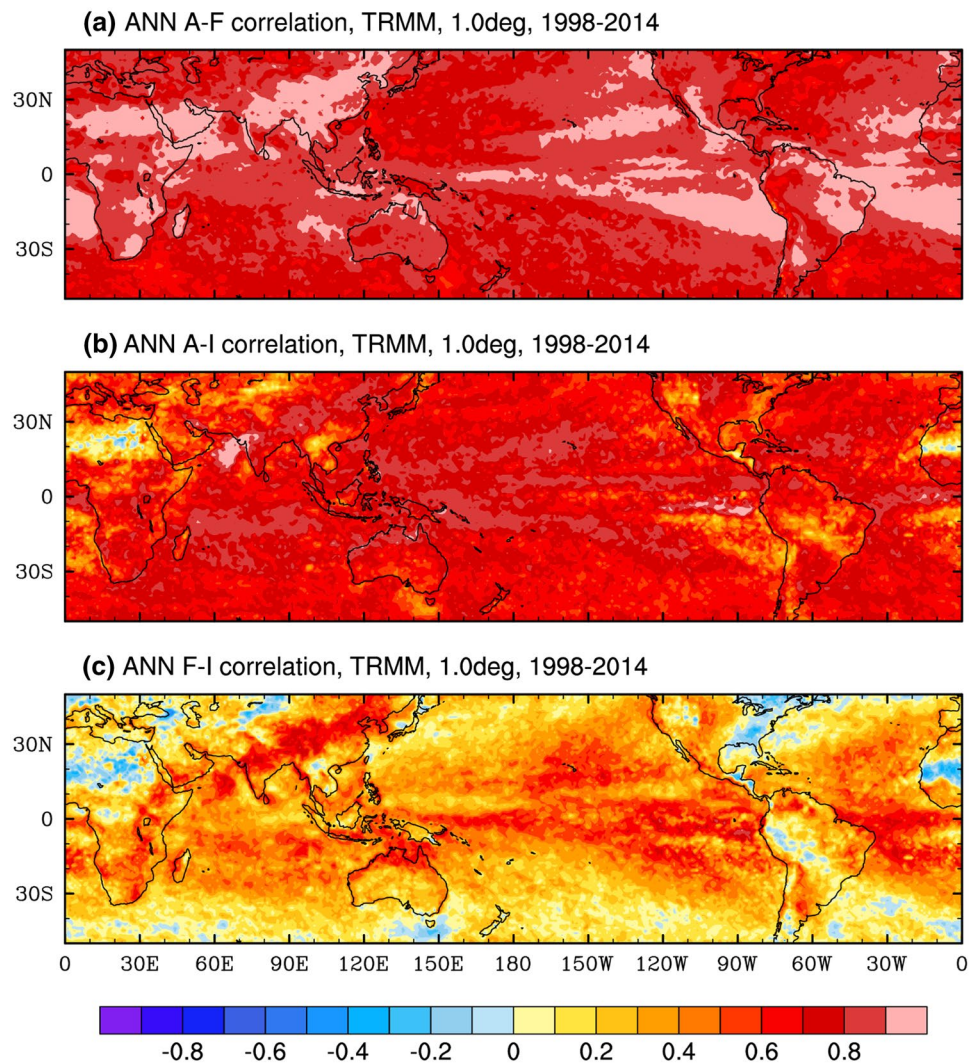
Thus, the frequency and intensity calculated using daily data are not comparable to those estimated using 3-hourly data.

Our simple relationship links the precipitation frequency estimated on a coarser grid or using data averaged over a longer period to that estimated on a finer grid or using data averaged over a shorter period. Tests using the TRMM 3B42 data showed that this simple relationship works well and suggests that the increase in the estimated frequency with the averaging grid size or time period is entirely due to the increased chance of precipitation as the area or time period increases. However, such increases do not simply follow the ratio of the averaging area or time of the input datasets, since precipitation is correlated in space and time (i.e., not purely random).

Despite the strong dependence on the resolution of the input data, the spatial patterns are similar among the precipitation frequency and intensity maps derived using data with different resolutions. The TRMM satellite data (on 0.25° grid) show extremely low frequency ($<1\%$) over the subtropical regions, and high frequency (20–40%) over the tropics (e.g. the ITCZ). Other land areas typically have a frequency below 10% (lower in winter and higher in summer). Further analyses revealed that the high frequency in the tropics and winter northern midlatitude storm track regions results from both longer and more frequent rain events, with the precipitation duration and event number showing spatial patterns similar to those of the frequency. The intensity is more uniformly distributed than the frequency, especially over the oceans, and its seasonal variations are also smaller than those of the frequency. Annual cycles of the zonal-mean precipitation amount, frequency and intensity suggest that seasonal frequency evolution resembles the amount more closely than the intensity, which is consistent with the notion that precipitation depends more on frequency than intensity. Year-to-year correlations also confirm that precipitation variability results more from frequency than intensity variations.

Our results highlight the importance of the data resolution in computing precipitation frequency and intensity. This is critical in comparisons of these two quantities between two datasets, or between observations and models, or among different models. As re-gridding of model precipitation involves spatial averaging, which alters the estimated precipitation frequency and intensity, we recommend to calculate the frequency and intensity on model's original grid, and simply average the high-resolution satellite data (without interpolation) onto a coarser grid that is closest to the model grid for comparison with the model statistics.

Fig. 17 Maps of local correlation between monthly anomalies (including all months) of precipitation: **a** amount and frequency, **b** amount and intensity, and **c** frequency and intensity based on TRMM 3B42 3-hourly precipitation data averaged onto 1° grid from 1998 to 2014



Acknowledgements The authors acknowledge the funding support from the U.S. National Science Foundation (Grant #AGS-1353740), the U.S. Department of Energy's Office of Science (Award No. DE-SC0012602), and the U.S. National Oceanic and Atmospheric Administration (Award No. NA15OAR4310086).

Appendix: A simple statistical relationship for the scale-dependence of precipitation frequency

What is the reason for the dependence of estimated precipitation frequency (F) and intensity (I) on the spatial and temporal resolution of the data used? Intuitively, larger grid boxes are more likely to capture some precipitation than smaller ones over a given time period (Kedem and Chiu 1987). For instance, a 0.5° grid box is four times larger than a 0.25° grid box, but the possibility of precipitation (i.e., precipitation frequency) is not four times larger for a 0.5° grid box than for a 0.25° grid box because precipitation events over different grid boxes are not independent

(e.g., they could occur at the same time over two or more 0.25° grid boxes within the 0.5° grid box), and they are often correlated spatially (Bell et al. 1990). Here, we aim to derive the relationship between the precipitation frequencies for a 0.25° grid box and a 0.5° grid box based on a pure probability consideration. The same kind of relationship applies for the dependence on temporal resolutions as well. In the following, we propose a simple statistical relationship based on basic probability concepts to explain the dependence of estimated precipitation frequency on the spatial and temporal resolutions of the data. The purpose of this exercise is two-folds: first to demonstrate that the frequency on two different grids are analytically linked and second to test whether the simple relationship we develop actually works as expected.

We first consider the dependence on the spatial resolution of the precipitation data. As illustrated in Fig. 18, the frequency of precipitation events for a coarse 0.5° grid box is related to the frequency for the finer 0.25° grid boxes inside it. Assuming the frequency (or probability) of

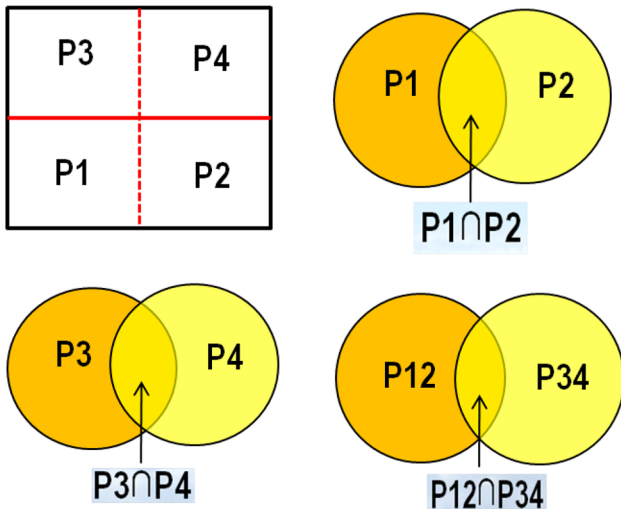


Fig. 18 A schematic diagram illustrating the overlapping (i.e., concurring) part of the precipitation events over two *small grid boxes* (denoted as P_1 – P_4) shown in the *top-left panel*. P_{12} and P_{34} represent the occurrence frequency for the *lower* and *upper part* of the *larger box*. The *circles* represent the occurrence frequency of precipitation events for each of the indicated *boxes*, and the overlapped area of the circles represent the concurring part of the frequency (i.e., the fractional times when precipitation happens over both *boxes*)

precipitation events for the small boxes are P_1 , P_2 , P_3 and P_4 (which can be calculated using the TRMM or CMORPH data), then the frequency for the lower two boxes (i.e., box 1 and 2 combined) is

$$P_{12} = P_1 \cup P_2 = P_1 + P_2 - P_1 \cap P_2 \quad (1)$$

where $P_1 \cap P_2$ is the overlapping frequency accounting for the events that occur in both box 1 and 2 at the same time. This frequency is included in both P_1 and P_2 and thus needs to be subtracted once from the sum. The same reasoning applies for the upper boxes (i.e., box 3 and 4 combined):

$$P_{34} = P_3 \cup P_4 = P_3 + P_4 - P_3 \cap P_4 \quad (2)$$

Similarly, the frequency for the big 0.5° grid box can be calculated as

$$P = P_{12} + P_{34} - P_{12} \cap P_{34} \quad (3)$$

Substitute Eqs. (1, 2) into Eq. (3), but use $P_{12} \cap P_{34} = (P_1 \cup P_2) \cap (P_3 \cup P_4)$ and $(a \cup b) \cap c = a \cap c + b \cap c - a \cap b \cap c$ to expand this term, we have

$$\begin{aligned} P = & (P_1 + P_2 + P_3 + P_4) \\ & - (P_1 \cap P_2 + P_1 \cap P_3 + P_1 \cap P_4 + P_2 \cap P_3 + P_2 \cap P_4 + P_3 \cap P_4) \\ & + (P_1 \cap P_2 \cap P_3 + P_1 \cap P_2 \cap P_4 + P_1 \cap P_3 \cap P_4 + P_2 \cap P_3 \cap P_4) \\ & - (P_1 \cap P_2 \cap P_3 \cap P_4). \end{aligned} \quad (4)$$

In Eq. (4), $P_1 \cap P_2 \cap P_3$ is for the frequency when precipitation occurs over all the 3 boxes at the same time (i.e., the frequency of joint occurrences), and similarly for the other terms with multiple “ \cap ”. These terms can be calculated directly using the data on the 0.25° grid. Thus, the precipitation frequency for a 0.5° box is analytically linked to the precipitation frequencies (P_1 to P_4 in Eq. 4) for the 0.25° boxes within the 0.5° box. We can use Eq. (4) and the frequencies (including the frequencies of joint occurrences) calculated using the TRMM or CMORPH data on a 0.25° grid to estimate the frequency on a 0.5° grid, and compare this estimate with that calculated directly using precipitation rates averaged onto the 0.5° grid. Strictly speaking, the threshold used to define the precipitation events should also be slightly different for the 0.25° and 0.5° cases if we want to use Eq. (4), except when it is zero. Thus, we will simply use a threshold of 0 mm/h in calculating the frequency on both the 0.25° and 0.5° grids using the TRMM 3B42 3-hourly data. The results are shown in Fig. 9 and discussed in Sect. 4.3.

Please note that Eq. (4) applies only to a special case where each grid box on the coarse grid contains exactly four grid boxes on the fine grid. The occurrence frequency terms on the fine grid boxes (P_1 , P_2 , P_3 and P_4) and the other terms of frequencies of joint occurrences in Eq. (4) will need to be calculated by counting the number of such events using the data on the fine grid (e.g., TRMM data on 0.25° grid). Thus these terms will depend on the actual data used.

We will apply similar reasoning to derive the equation linking the frequencies for two different temporal resolutions, namely, for 3-hourly and daily data. Replacing each small box in Fig. 18 with a 3-h time period, and considering the big box as the 12-h period consisting of the four 3-h periods, then Eq. (4) can be used to calculate the frequency over the 12-h period using the frequency calculated using 3-hourly data. The same method can be applied to the other 12-h period of the day. Following the same reasoning, the frequency or probability for the whole day (P) can be estimated as

$$P = P_{1234} + P_{5678} - P_{1234} \cap P_{5678} \quad (5)$$

where P_{1234} and P_{5678} are, respectively, the frequency for the first (i.e., 00–03, 03–06, 06–09 and 09–12Z) and second (i.e., 12–15, 15–18, 18–21 and 21–24Z) 12-h periods calculated using Eq. (4) and the frequencies estimated using 3-hourly data. The last term in Eq. (5) (i.e., $P_{1234} \cap P_{5678}$) represents the overlapped frequency for the first and second 12-h periods, and we will estimate it directly using 12-hourly averaged precipitation rates by computing their concurring frequency. Thus, Eq. (5) links the daily precipitation frequency to the precipitation frequency estimated using 3-hourly (and 12-hourly) precipitation rates. This

estimate from Eq. (5) can be compared with that calculated directly from daily mean precipitation rates (both on the same grid). For this comparison, we will again use zero as the threshold to simplify the definition of precipitation events. The results are shown in Fig. 10 and discussed in Sect. 4.3.

References

- Arkin PA (1979) The relationship between the fractional coverage of high cloud and rainfall accumulations during GATE over the B-array. *Mon Weather Rev* 107:1382–1387
- Bell TL, Abdullah A, Martin RL, North GR (1990) Sampling errors for satellite-derived tropical rainfall: Monte Carlo study using a space-time stochastic model. *J Geophys Res* 95:2195–2205
- Biasutti M, Yuter SE (2013) Observed frequency and intensity of tropical precipitation from instantaneous estimates. *J Geophys Res* 118:9534–9551
- Biasutti M, Yuter SE, Burleyson CD, Sobel AH (2011) Very high resolution rainfall patterns measured by TRMM precipitation radar: seasonal and diurnal cycles. *Clim Dyn* 39:239–258
- Chen M, Dickinson RE, Zeng X, Hahman AN (1996) Comparison of precipitation observed over the continental United States to that simulated by a climate model. *J Clim* 9:2233–2249
- Dai A (2001a) Global precipitation and thunderstorm frequencies. Part I: Seasonal and interannual variations. *J Clim* 14:1092–1111
- Dai A (2001b) Global precipitation and thunderstorm frequencies. Part II: diurnal variations. *J Clim* 14:1112–1128
- Dai A (2006) Precipitation characteristics in eighteen coupled climate models. *J Clim* 19:4605–4630
- Dai A, Fung IY, Del Genio AD (1997) Surface observed global land precipitation variations during 1900–1988. *J Climate* 10:2943–2962
- Dai A, Giorgi F, Trenberth KE (1999) Observed and model simulated precipitation diurnal cycle over the contiguous United States. *J Geophys Res* 104:6377–6402
- Dai A, Lin X, Hsu K (2007) The frequency, intensity, and diurnal cycle of precipitation in surface and satellite observations over low- and mid-latitudes. *Clim Dyn* 29: 727–744
- Dai A, Rasmusson RM, Liu C, Ikeda I, Prein AF (2017) A new mechanism for warm-season precipitation response to global warming based on convection-permitting simulations. *Clim Dyn.* doi:[10.1007/s00382-017-3787-6](https://doi.org/10.1007/s00382-017-3787-6)
- DeMott CA, Randall DA, Khairoutdinov M (2007) Convective precipitation variability as a tool for general circulation model analysis. *J Clim* 20:91–112
- Deng Y, Bowman KP, Jackson C (2007) Differences in rain rate intensities between TRMM observations and community atmosphere model simulations. *Geophys Res Lett* 34:L01808
- Ellis TD, L'Ecuyer T, Haynes JM, Stephens GL (2009) How often does it rain over the global oceans? The perspective from Cloud-Sat. *Geophys Res Lett* 36:L03815. doi:[10.1029/2008GL036728](https://doi.org/10.1029/2008GL036728)
- Gehne M, Hamill TM, Kiladis GN, Trenberth KE (2016) Comparison of global precipitation estimates across a range of temporal and spatial scales. *J Clim* 29:7773–7795
- Higgins RW, Janowiak JE, Yao YP (1996) A gridded hourly precipitation data base for the United States (1963–1993). US Department of Commerce, National Oceanic and Atmospheric Administration, National Weather Service
- Huffman GJ, Adler RF, Bolvin DT, Gu G, Nelkin EJ, Bowman KP, Hong Y, Stocker EF, Wolff DB (2007) The TRMM multisatellite precipitation analysis (TMPA): quasi-global, multiyear, combined-sensor precipitation estimates at fine scales. *J Hydrometeorol* 8:38–55
- Huffman GJ, Adler RF, Bolvin DT, Gu GJ (2009) Improving the global precipitation record: GPCP version 2.1. *Geophys Res Lett* 36:L17808
- Joyce RJ, Janowiak JE, Arkin PA, Xie P (2004) CMORPH: A method that produces global precipitation estimates from passive microwave and infrared data at high spatial and temporal resolution. *J Hydrometeorol* 5(3):487–503
- Kedem B, Chiu LS (1987) Are Rain Rate Processes Self-Similar? *Water Resources Res* 23:1816–1818
- Kedem B, Chiu LS, Karni Z (1990) An analysis of the threshold method for measuring area-averaged rainfall. *J Appl Meteor* 29:3–20
- Lau WKM, Wu HT (2007) Detecting trends in tropical rainfall characteristics, 1979–2003. *Int J Climatol* 27:979–988
- Lau WKM, Wu HT, Kim KM (2013) A canonical response of precipitation characteristics to global warming from CMIP5 models. *Geophys Res Lett* 40:3163–3169
- Liu Z (2015) Comparison of versions 6 and 7 3-hourly TRMM multisatellite precipitation analysis (TMPA) research products. *Atmos Res* 163: 91–101
- Liu SC, Fu C, Shiu CJ, Chen JP, Wu F (2009) Temperature dependence of global precipitation extremes. *Geophys Res Lett* 36:L17702
- Lu E, Ding Y, Zhou B, Zou X, Chen X, Cai W, Zhang Q, Chen H (2016) Is the interannual variability of summer rainfall in China dominated by precipitation frequency or intensity? An analysis of relative importance. *Clim Dyn* 47:67–77
- Ma S, Zhou T, Dai A, Han Z (2015) Observed changes in the distributions of daily precipitation frequency and amount over China from 1960 to 2013. *J Clim* 28:6960–6978
- Pendergrass AG, Hartmann DL (2014a) Changes in the distribution of rain frequency and intensity in response to global warming. *J Clim* 27:8372–8383
- Pendergrass AG, Hartmann DL (2014b) The atmospheric energy constraint on global-mean precipitation change. *J Clim* 27:757–768
- Petty GW (1995) Frequencies and characteristics of global oceanic precipitation from shipboard present-weather reports. *Bull Am Meteorol Soc* 76:1593–1616
- Petty GW (1997) An intercomparison of oceanic precipitation frequencies from 10 special sensor microwave/imager rain rate algorithms and shipboard present weather reports. *J Geophys Res* 102(D2):1757–1777
- Qian T, Dai A, Trenberth KE, Oleson KW (2006) Simulation of global land surface conditions from 1948 to 2004. Part I: Forcing data and evaluation. *J Hydrometeorol* 7:953–975
- Shiu CJ, Liu SC, Fu C, Dai A, Sun Y (2012) How much do precipitation extremes change in a warming climate? *Geophys Res Lett* 39:L17707
- Sun Y, Solomon S, Dai A, Portmann R (2006) How often does it rain? *J Clim* 19:916–934
- Sun Y, Solomon S, Dai A, Portmann R (2007) How often will it rain? *J Clim* 20:4801–4818
- Trenberth KE (2011) Changes in precipitation with climate change. *Clim Res* 47: 123–138
- Trenberth KE, Dai A, Rasmusson RM, Parsons DB (2003) The changing character of precipitation. *Bull Am Meteorol Soc* 84:1205–1217
- Xie P, Joyce RJ (2014) Integrating information from satellite observations and numerical models for improved global precipitation analyses: exploring for an optimal strategy. *Remote Sensing of the Terrestrial Water Cycle. Geophys Monogr Am Geophys Union* 206:43–60, doi:[10.1002/9781118872086.ch3](https://doi.org/10.1002/9781118872086.ch3)
- Xie P, Joyce R, Wu S, Yoo S-H, Yaroah Y, Sun F, Lin R (2017) Reprocessed, bias corrected CMORPH global high-resolution

- precipitation estimates. *J Hydromet.* doi:[10.1175/JHM-D-16-0168.1](https://doi.org/10.1175/JHM-D-16-0168.1). (In press)
- Zhou TJ, Yu RC, Chen HM, Dai A, Pan Y (2008) Summer precipitation frequency, intensity, and diurnal cycle over China: a comparison of satellite data with rain gauge observations. *J Clim* 21:3997–4010
- Zipser EJ, Liu C, Cecil DJ, Nesbitt SW, Yorty DP (2006) Where are the most intense thunderstorms on Earth? *Bull Am Meteorol Soc* 87:1057–1071